Immediate *In Situ* Identification of Gram-negative Bacteria in Human Lungs Using a Topical Fluorescent Peptide Targeted Against Lipid A

Ahsan R Akram[1,2], Sunay V Chankeshwara[1,3], Emma Scholefield[1], Tashfeen Aslam[3], Neil McDonald[2], Alicia Megia-Fernandez[1,3], Adam Marshall[1,2], Beth Mills[1], Nicolaos Avlonitis[3], Marc Vendrell[2], Thomas H Craven[1,2], Annya M Smyth[1], David S Collie[4], Calum Gray[5], Nik Hirani[2], Adam T Hill[2], John R Govan[6], Timothy Walsh[1,2], Christopher Haslett[1,2], Mark Bradley*[1,3] & Kevin Dhaliwal*[1,2].

Affiliations:

[1] EPSRC IRC PROTEUS Hub, MRC Centre for Inflammation Research, Queen's Medical Research Institute, University of Edinburgh, 47 Little France Crescent, Edinburgh, United Kingdom, EH16 4TJ.

[2] MRC Centre for Inflammation Research, Queen's Medical Research Institute, University of Edinburgh, 47 Little France Crescent, Edinburgh, United Kingdom, EH16 4TJ.

[3] EaStCHEM, The University of Edinburgh School of Chemistry, Joseph Black Building, West Mains Road, Edinburgh, United Kingdom, EH9 3FJ.

[4] The Roslin Institute and R(D)SVS, University of Edinburgh, Easter Bush Veterinary Centre, Roslin, Midlothian, United Kingdom.

[5] Clinical Research Imaging Centre, Queen's Medical Research Institute, University of Edinburgh, 47 Little France Crescent, Edinburgh, United Kingdom, EH16 4TJ.

[6] Division of Infection and Pathway Medicine, University of Edinburgh, The Chancellor's Building, 49 Little France Crescent, Edinburgh, United Kingdom, EH16 4SB.

.

*** To whom correspondence should be addressed: Professor Kev Dhaliwal & Professor Mark Bradley, Pulmonary Optical Molecular Imaging Group, MRC Centre for Inflammation Research, Queen's Medical Research Institute, 47 Little France Crescent, Edinburgh, United Kingdom, EH16 4TJ. Email: Kev.Dhaliwal@ed.ac.uk and Mark.Bradley@ed.ac.uk**

One Sentence Summary: A topically administered fluorescently labelled peptide targeted against Lipid A permits the real-time visualization of bacteria in the distal lung of humans within 60 seconds of administration.

Abstract: Respiratory infections in mechanically ventilated patients caused by gram-negative bacteria are a significant cause of morbidity and antibiotic administration. Current methodologies are unable to rapidly and unequivocally determine the presence, localization or abundance of bacteria in the distal lung to aid in the diagnoses of bacterial pneumonia, stratify patients for antibacterial therapy and monitor treatment efficacy. Here, we describe an *in situ* visualization methodology combining the imaging of cellular infiltrates and gram-negative bacterial species in the distal human lung which is achieved by combining autofluorescence optical endomicroscopy with an optical imaging probe based on the antimicrobial peptide polymyxin conjugated to an environmentally sensitive fluorophore. This SmartProbe is water soluble, chemically stable, non-toxic and after in-human intrapulmonary microdosing, enables the specific detection of gram-negative bacteria in the distal human airways and alveoli within sixty seconds. This first-in-human pilot study shows that pulmonary molecular imaging using a topically administered fluorescent SmartProbe specific for Lipid-A is safe and practical, enabling the immediate *in situ* identification of gram-negative bacteria in humans. This is the first description of identification of bacteria in humans by optical molecular imaging.

Introduction

Gram-negative pulmonary infection (GNPI) is a frequent and severe consequence of hospitalization, immunosuppression and mechanical ventilation(*1*). However, the accurate and rapid diagnosis of gram-negative pneumonia is challenging and the monitoring of antimicrobial efficacy *in vivo in situ* is currently not feasible. The gold standard diagnostic *in situ* procedure for pneumonia (defined as infection in the gas-exchanging regions of the human lung alongside a host cellular response), remains biopsy and culture(*2, 3*). However, biopsy is rarely performed as a diagnostic tool for pneumonia, and would have safety concerns if performed in mechanically ventilated patients.

Consequently, new pulmonary infiltrates on chest x-ray in mechanically ventilated patients often lead to broad spectrum antimicrobial administration, as the clinical suspicion of nosocomial pneumonia is overly sensitive(*4*). Current approaches to guide antimicrobial therapy for suspected pneumonia rely on the growth of bacteria from aspirated fluids or expectorated samples alongside antimicrobial susceptibility testing(*4-6*). In mechanically ventilated patients and immunosuppressed lung transplant patients, bronchoalveolar lavage (BAL) is a routinely used sampling methodology. However, BAL has suboptimal specificity and sensitivity(*7*) and is associated with significant delays as culture results take up to 72 hours(*8*). Furthermore, although BAL aims to sample the alveolar space, it is invariably contaminated by tracheobronchial organisms resulting in low specificity(*4, 9*) and subsequent over-treatment; similarly, negative culture results from distal airways sampling may lack validity as a result of concurrent antimicrobial therapy(*10*) or poor sampling(*5, 11, 12*). Conversely, molecular techniques such as polymerase chain reaction (PCR) that employ amplification and sequencing of potential microbial species in expectorated or sampled fluids are inherently over sensitive(*13*).

Given these inherent limitations of existing approaches, an *in situ* methodology for the rapid and accurate identification of GNPI has potential benefits. Hence, the aim of this study was to develop and test the feasibility, in humans for the first time, an optical molecular imaging (OMI) approach combining intrapulmonary delivery of a SmartProbe specific for the presence of Gram-negative bacteria and optical endomicroscopy (OEM) of the distal lung to observe both autofluorescent cellular infiltrates and bacterial presence. This has the potential to provide *in situ* molecular imaging of specific bacteria

in humans as a diagnostic and monitoring tool and also a technology platform to increase understanding of human-microbial pathology. To demonstrate proof-of-concept in a first-in-human study, we selected six patients with chronic pulmonary infection to show specificity of the approach, followed by a small cohort of critically ill mechanically ventilated patients in the intensive care unit (ICU) who had suspected pneumonia and were scheduled for a bronchoalveolar lavage for diagnostic purposes. The cohorts represented patients in whom gram-specific colonization of bacteria was likely (bronchiectasis) to provide proof of concept of specificity in humans and in patients in whom de novo ventilator-associated pneumonia (VAP) was suspected (ICU) to provide proof-of-concept and early feasibility of diagnostic utility prior to embarking upon larger scale diagnostic validation studies.

We investigated the utility of Polymyxins (PMXs) as a selective binding ligand for gram-negative bacteria. PMXs are naturally occurring cationic, amphipathic, cyclic antimicrobial peptides, formed by the bacterium *Paenibacillus polymyxa*(*14, 15*) and bind to Lipid A of lipopolysaccharide (LPS) on the outer membrane of gram-negative bacteria(*16, 17*). We synthesized a library of fluorescently labelled PMX derivatives labelled with an environmentally sensitive fluorophore, 7-nitrobenz-2-oxa-1,3-diazole (NBD), generating excellent signal-to-noise ratios with fluorescent amplification only upon entry into the hydrophobic environment of the bacterial membrane. The lead optimized SmartProbe, NBD-PMX was evaluated; *in vitro* against a panel of clinical bacterial isolates and primary human cells, in an *ex vivo* ventilated ovine lung model and in preclinical toxicology models. NBD-PMX was manufactured to good manufacturing practice (GMP) for a first-in-human study in six patients with established distal lung bacterial presence (bronchiectasis) and in seven patients with suspected pneumonia in the ICU to rapidly (within sixty seconds) and specifically visualize autofluorescent cellular infiltrates and gram-negative bacteria in the distal lung with OEM. This is the first report of specific and sensitive immediate *in vivo in situ* imaging of bacteria in humans.

Results

Structure-activity relationship of NBD-PMX constructs demonstrate an optimal SmartProbe to selectively label gram-negative bacteria with high signal-to-noise in alveolar tissue

A panel of modified Polymyxin B constructs was chemically synthesized and evaluated for specificity against *Pseudomonas aeruginosa* and *Staphylococcus aureus*. Polymyxin B was modified by removal of the hydrophobic tail and two amino acid residues and replaced with various linkers attached to the fluorophore NBD (without alteration of cyclic ring component). Progressive lengthening of linker led to loss of gram selectivity (fig. S1). The lead compound (fig. 1A) with an amino-PEG2-carboxylate spacer showed fluorescence amplification in increasingly non-polar environments, demonstrating the required environmental reporting for optimal fluorescence amplification upon bacterial membrane insertion (fig. 1B) and labelled *P. aeruginosa,* in a concentration dependent manner with high signal-to-noise (fig. 1C).

Gram selectivity was assessed against a broad and clinically relevant panel of organisms and demonstrated labelling selectivity for gram-negative bacterial species; *Pseudomonas aeruginosa, Klebsiella pneumoniae, Escherichia. coli, Haemophilus influenzae, Acinetobacter baumannii* and *Stenotrophomonas maltophilia* but not for gram-positive bacterial species; Methicillin sensitive *Staphylococcus aureus*, Methicillin resistant *S. aureus* and *Streptococcus pneumoniae* (fig. 1D-F). To demonstrate selectivity over mammalian cells, NBD-PMX was imaged in co-culture with freshly isolated human peripheral blood granulocytes and mononuclear cells and also with alveolar macrophages retrieved from BAL (fig. 2A-C). Furthermore, there was no labelling of human lung epithelial cells demonstrated in a bacterial-human lung co-culture (fig. 2D) while low concentrations of NBD-PMX preferentially labelled bacteria in the presence of pulmonary surfactant (fig. S2).

To determine its mode of action, the *Burkholderia cenocepacia* strain K56-2, which is highly resistant to Polymyxin B through mutations in its Lipid A component(*18, 19*) was treated with the NBD-PMX probe. This showed a lack of binding, suggesting that NBD-PMX labelling of gram-negative bacteria is through Lipid A binding (fig. S3).

NBD-PMX demonstrated no toxicity and chemical stability

NBD-PMX demonstrated no membrane toxicity in an *in vitro* haemolysis assay and no toxicity or pulmonary inflammatory cell recruitment after intratracheal instillation in mice (fig. S4). This was confirmed by a contract research organization good laboratory practice (GLP) rat single-dose intratracheal toxicology study (with over 600 times the human dose based on lung weight) where no significant changes in weight, haematological, coagulation and clinical chemistry parameters were observed (table S1). Furthermore, no adverse pathological observations were noted between the two groups at day 3 or day 15 in lung, liver, kidney or reproductive organs.

NBD-PMX was manufactured to GMP and stability studies (24 months) demonstrated chemical stability of the aqueous drug product under frozen (-20^0C) storage conditions. (table S2).

NBD-PMX visualizes gram-negative bacterial bioburden in the distal lung with topical microdosed endobronchial delivery and OEM in a large animal ex vivo lung model

An important technical prerequisite of the approach required evidence that bacteria could be rapidly detected in the distal alveolar regions with a clinically-relevant limit of detection (LoD) and sampling methodology. An ovine *ex vivo* whole lung ventilated model of distal lung bacterial burden was developed which facilitated evaluation of NBD-PMX against a diverse panel of clinically relevant pathogenic bacteria in a human-size-relevant lung model (fig. 3A). This model allowed the use of clinical equipment and the thorough testing of the technical feasibility of delivering microdoses (<100 mcgs) of NBD-PMX and detection of labelled bacteria in distinct bronchopulmonary segments after regional OEM. OEM enables the delineation between bronchiolar imaging and alveolar imaging through the very distinct autofluorescence patterns of elastin. The presence and distribution of bacteria were initially modelled *in situ* with the instillation of GFP *S. aureus* which demonstrated a characteristic imaging pattern of punctate twinkling bacteria (movie S1). Anatomically distinct bronchopulmonary segments were instilled with bacteria or vehicle control and subsequently microdoses of NBD-PMX were instilled and lung segments were immediately imaged using OEM. This was achieved by passing an OEM fibre into disparate bronchopulmonary segments (up to 5 passes per bronchopulmonary

segment to capture a regional representation of fluorescence), recording images at 12 frames per second and imaging for up to 5 minutes. The regional exploration of the bronchopulmonary segments was intended to mimic the clinical scenario of performing sampling in bronchopulmonary segments guided by chest x-ray infiltrates. It was demonstrated that this approach can detect gram-negative bacteria, but not gram-positive or control segments (fig. 3B-C). A simple image analysis algorithm was developed to objectively detect bacteria and analyze and quantify the videos on a frame-by-frame basis, thus confirming the ability of NBD-PMX to discriminate gram-negative bacteria from gram-positive and buffer control segments (fig. 3D-F) with bacteria visualized within 60 seconds of instillation. The imaging algorithm was developed to discriminate a clinically relevant LoD of $1x10^5$ colony forming units/ml in BAL. To observe if it was feasible to clearly distinguish various bioburdens of bacteria with this approach, different concentrations of *E. coli* were instilled and imaging performed as described above. Using the developed algorithm, ranges of $1x10^5$ to $1x\ 10^9$ bacterial bioburden in the distal alveoli were clearly distinguishable (fig. S5).

NBD-PMX enables immediate in situ visualization of gram-negative bacteria in the distal lung of bronchiectasis patients

Bronchiectasis is a chronic suppurative pulmonary disease characterized by distal lung bacterial colonization and repeated infective exacerbations(*20*) with pathogens, often gram-negative, that are commonly found in mechanically ventilated patients and patients who receive lung allografts. Thus GMP manufactured NBD-PMX was topically administered as a microdose via an intrapulmonary catheter during a bronchoscopy procedure to six patients with bronchiectasis with imaging of the distal airways and alveoli initiated within sixty seconds. The distal airways of interest were determined *a priori* by a computed tomography. Four females and two males with a mean age of 65 comprised the study population and no patient had a serious adverse event (table S3). Minor adverse events such as cough attributable to the bronchoscopy procedure were observed in three patients. BAL and sputum culture was performed after the imaging procedure and bacterial species identified. The imaging videos obtained following NBD-PMX demonstrated the very clear presence (or absence) of gram-negative bacteria by the the human observer (movies S2-7).

Furthermore, using an image analysis algorithm analogous to that used in the ovine *ex vivo* model, bacterial signal was considered positive or negative based upon an algorithm measuring the increase in punctate signal pre and post administration of the NBD-PMX (fig. 4). The deployment of an arbitrary cut off clearly distinguished positive from negative frames (fig. 4).

Negative bacterial signal was seen in three patients: D1, D3 and D4. Upon culture, patients D1 and D3 grew only a gram-positive organism and D4 grew a PMX resistant gram-negative organism (*Proteus miribalis*) (fig. 4 and movies S2, S4 and S5). Striking positive bacterial signals were seen in D2, D5 and D6. D2 and D5 grew *P. aeruginosa*, (fig. 4 and movies S3 and S6), while D6 grew two different species; *S. pneumoniae* and *H. influenzae* Therefore, this positive signal was attributed to *H. influenzae* presence.

Interestingly, bacterial signals were clearly observed in the distal alveolar regions, which conventionally are considered to be low in bacterial bioburden in chronic suppurative lung disease at post-mortem(*21*). Unsurprisingly, bacterial aggregates were observed in the distal bronchioles of these patients (figure S6).

NBD-PMX and OEM enable immediate in situ visualization of gram-negative bacteria and cellular infiltrates in the distal lung of ICU patients

We then performed the procedure in seven ICU patients with suspected pneumonia to demonstrate early feasibility, assess safety and to discern in an unselected cohort if a qualitative signature of infection in the distal alveoli could be observed. One patient (D10) was excluded from the analysis as no videos could be analysed and no BAL was retrieved, however this patient demonstrated no study related adverse events. The six patients in whom imaging and BAL analysis was performed provided initial proof-of-concept in whom there was the possibility of a gram-negative VAP (table S4). No study related serious adverse events were noted and the average procedure time (including BAL) was 14.7 minutes with 4.8 passes in the endobronchial segments imaged. Two patients, D7 and D11 (fig 5 and movie 8 and 11), demonstrated a characteristic bacterial signal and both also demonstrated an autofluorescent cellular infiltrate. BAL yielded no significant bacterial growth for patient D7, which was unsurprising

as the patient was on multiple antimicrobials including metronidazole, ciprofloxacin, vancomycin and the anti-fungal fluconazole for a perforated abdominal viscus. BAL from patient D11 demonstrated growth of the gram-negative bacteria *Klebsiella oxytoca* at low levels (table S4) (BAL microbial culture was suppressed by the prior administration of intravenous teimocillin) and the fungus *Candida albicans*. *Ex vivo* labelling of BAL from D11 with NBD-PMX demonstrated labelling of *Klebsiella oxytoca* but not *Candida albicans* (fig S7). Patients D8 and D13 demonstrated no bacterial labelling and no inflammatory cellular infiltrate in the alveoli, but did demonstrate the absence of well-aerated alveoli, as there were condensed/compressed elastin structures (fig 5. and movie 9 and 13) consistent with atelectasis of the segment. Growth of *S. maltophilia* was demonstrated for D8 in both tracheal aspirates prior to procedure, and on BAL at $1x10^4$ CFU/ml. Given the absence of distal alveolar bacterial signal and the absence of a cellular infiltrate, this was attributed to airway colonisation. Patient D9 and D12 both demonstrated no distal alveolar bacteria, no cellular infiltrate and BAL grew bacteria below the threshold for VAP, consistent with absence of VAP. Patient D12 developed a pulmonary abscess prior to imaging, which was additionally identified on OEM by the absence of elastin autofluorescence.

Whilst these are preliminary studies in an unselected cohort of critically ill patients with new pulmonary infiltrates on CXR, they demonstrate the early feasibility of this point-of-care technology platform and also the utility of a qualitative imaging signature of alveolar cellular infiltrate and bacterial presence.

Discussion

The inexorable rise of antimicrobial resistance (AMR) has in part been driven by the indiscriminate administration of antibiotics to individuals suspected of having infections. Upper airway and bronchoscopic sampling and subsequent microbiological culture are routinely used in mechanically ventilated patients and also in patients who have received lung allografts. However, these diagnostic approaches have limited sensitivity and specificity and also significant delays in reporting, such that empirical antibiotic therapy is frequently initiated leading to inappropriate and/or overtreatment with broad-spectrum antibiotics. Empirical antibiotic therapy is associated with increased morbidity, exposes patients to potential drug toxicity, promotes AMR, increases the risk of antibiotic-associated infections and wastes health service resource. Moreover, there is no robust method to guide cessation or refinement/de-escalation of antimicrobial therapy. Therefore, technologies that enable bacterial detection, bacterial bioburden and bedside qualitative measure of pulmonary infection in the distal lung may have significant utility. Molecular imaging of infection in humans has been dominated by nuclear medicine approaches and whilst these do offer whole-body imaging, they are expensive, cumbersome, limited to large centers, are not point-of-care, offer poor specificity and variable sensitivity(*22*) and have not been adopted. Indeed, using whole-body approaches, it is impossible to delineate true distal lung alveolar infection from tracheobronchial colonization and in the specific case of mechanically ventilated patients, adds significant time, safety and often transport challenges as critically-ill patients need to be moved to the scanners.

Although there have been significant technical developments in developing bacterial OMI for small animals or tissue explants(*23-26*), to date, there have been no reports of clinical translation. Partnering intrapulmonary microdosed SmartProbes with OEM is a platform technology enabling molecular imaging of the distal lung at high resolution, with the potential for serial exploration of pulmonary segments. The distal airway and alveolar elastin networks allow clear visualization of the spatial location within the lung through autofluorescence imaging at 488nm excitation(*27*). Importantly, the OEM fibre is only extended through the working channel of the bronchoscope once it is wedged in the distal lung. This simple method avoids proximal tracheobronchial contamination which is a major issue

with existing methods. The targeting nature of the NBD-PMX coupled with selected distal lung optical imaging ensures potentially high specificity with this approach and coupling this with the imaging signature of a cellular infiltrate has the added potential to be more predictive of alveolar infection vs colonization. The true signature of infection vs colonization requires larger studies with further evaluation compared to accepted reference standards.

In clinical practice, PMX isomers are used as antimicrobial agents(*28, 29*), hence we chose to use PMX as a binding ligand for OMI. PMX was linked to an environmentally sensitive fluorophore to allow signal generation only upon bacterial membrane engagement and generation of high signal-to-noise when administered topically into the human lung. Any potential toxicity concerns were obviated by the absence of *in vitro* and *in vivo* toxicity and the miniscule (100mcg) mass that was delivered directly into the distal lung.

Salient chemical modifications of Polymyxin B enabled specific and sensitive gram-negative bacterial molecular imaging. Importantly, we retained the positively charged diaminobutyric-acid (DAB) residues on the cyclic ring which are important for overall cationic charge(*30*) and bacterial binding. We removed the membrane perturbing hydrophobic tail containing fatty acid chains and one amino acid residue (and replaced these with a hydrophilic PEG spacer and the relatively hydrophobic NBD fluorophore. Structure–activity relationship studies showed that the linker length between the PMX and NBD was crucial for binding, while the the amphipathic properties of NBD-PMX were maintained by the hydrophobic residues which remained in position 6 and 7 (D-phe and Leu respectively)(*17*). We confirmed that the binding of NBD-PMX was Lipid A mediated by demonstrating absence of binding to a Lipid A mutant *B. cenocepacia* isolate (mechanisms of PMX resistance remain largely confined to alterations to the Lipid A component of LPS(*31, 32*)). Currently, PMX resistance in nosocomial gram-negative infections is rare, even amongst multi-drug resistance strains(*29, 33, 34*), such that NBD-PMX will have wide applicability.

As a proof-of-concept, we initially demonstrated that microdoses of NBD-PMX administered endobronchially, specifically bind to gram-negative bacteria and enable immediate visualization of

bacteria in the distal *ex vivo* ovine lung by OEM. It was clear to the observer whether Gram-negative bacteria were present or absent within seconds. We further demonstrated that a defined sampling strategy and a bespoke objective imaging analysis algorithm to detect punctate bacterial signal had excellent performance.

To extend the possibility of using such a technology platform to monitor treatment response, bioburden of bacteria in the distal lung was clearly distinguishable. Due to rising multidrug resistance, GNPI is emerging as one of the most difficult infections to treat due to rising multidrug resistance(*35*, *36*) and the evaluation of existing and new improved antimicrobial regimes is hindered by poor surrogate markers of efficacy, thus the ability for repeated visualization of bacterial bioburden in the distal lung to serially monitor pathogen bioburden may help to refine/escalate and deescalate therapy. Although the use of OEM has been demonstrated to be safe, repeated visualization does require repeat bronchoscopy and consequently the associated risks of repeated use of this technology will need to be weighed against the information it could provide.

In the clinical study, it was instantaneously clear to the clinician, whether the signal was positive or negative; In the six bronchiectasis patients, we clearly observed Gram-specific imaging of bacteria and in the ICU patients we observed qualitative signatures of infection in two patients. Clinical adoption and future use of such platforms requires large well-constructed trials to demonstrate efficacy and safety alongside health economic evaluation. The challenge of distinguishing de novo bacterial infection vs resolving infection or indeed colonization is an important clinical question and necessitates novel technology development. The technology platform that we have developed, now requires a large multi-site phase 2 validation study based upon STARD guidelines(*37*). At this stage of development, the technology has demonstrated safety and feasibility in the ICU, but follow on studies to determine diagnostic accuracy will require appropriately powered recruitment of suspected pneumonia in over 300 ICU patients. These multicenter studies will be essential to support the utility of this approach and in improving and validating the imaging signature with further refinements of the algorithms.

Regarding clinical applicability, currently, the fibre optic confocal fibres cost $300-400 per procedure and are restricted to limited uses and require sterilization between uses. These costs are significant due to the source of optical multicore fibres from manufacturers that use expensive preforms. However, single use low-cost disposable fibres, which dramatically reduce this cost have now been developed (*38*) which will reduce the cost to $5 per procedure. Similarly, the cost of goods of the imaging SmartProbes is low and with the advent of frugal innovation and technology such as widefield OEM(*39*), this approach is potentially cost-effective.

Whilst GNPI are the predominant cause of pulmonary infections in lung transplantation(*40*) and in nosocomial infections in the ICU(*41*), pneumonia may be caused by gram-positive or multiple bacterial species(*42*). Hence in the longer term, this diagnostic platform will require a matching gram-positive imaging agent, such as fluorescently label Vancomycin(*26*) or other gram-positive selective ligands, or alongside other bacterial SmartProbes(*43*) as OEM has the potential to be multiplexed(*22, 39*). It is also feasible to exploit other properties to further distinguish bacterial labelling from intrinsic lung autofluorescence such as fluorescence lifetime imaging or a spectrally distinct fluorophore. In this small clinical study, NBD-PMX did not detect *Proteus Mirabilis* which is known to be PMX-resistant. *P. mirabilis* is an uncommon cause of nosocomial pneumonia(*41*) and opportunistic pulmonary infection in immunosuppressed patients, it did however show the potential of the platform to detect AMR.

This proof-of-concept study was to determine if Gram-negative bacteria could be labelled *in situ* in the distal human lung; consequently, although our ICU cohort demonstrates significant promise in this regard, larger studies are needed to fully address the distinction between colonization or true infection with this modality. However, the absence of a true gold standard for bacterial infection in the mechanically ventilated patient, makes this challenging. Nevertheless, as demonstrated, high resolution OEM coupled with SmartProbes was able to delineate bacterial presence in distinct segments of the pulmonary tree (such as the acinar gas exchanging unit) and associated imaging parameters such as cellular infiltrates. To our knowledge, this is the first in-human report of bacterial visualization *in situ* in the human lung. The specificity, safety, rapidity, low cost and rapid readout of this technology

platform represent potentially significant advantages over current technologies, and now require further large scale validation.

Methods

Ethics Statement: All experiments using human samples *in vitro* were performed following approval of the appropriate regional ethics committee (REC) and with informed consent of the patients. BAL for alveolar macrophages: (REC no: 07/S1102/20), blood for isolation of neutrophils and mononuclear cells: (REC no: 08/S1103/38) and human lung tissue: (REC no: 13/ES/0126). Animal experiments were performed under UK Home Office Animals Scientific Procedures Act 1986 (Project License Number 60/4434). Ovine lungs were from ewes destined for cull and were euthanized under Schedule 1 of Animals (Scientific Procedures) Act 1986. The *in vivo* clinical study (ClinicalTrials.gov identifier: NCT02491164) was approved by Regional Ethics Committee (REC no: 15/SS/0126) and informed consent was taken from all patients.

Chemical synthesis: Details of the synthetic pathway for NBD-PMX are provided in the Supplementary information.

Bacterial Culture: Bacterial strains were grown and counterstained as previously described(*43*). Strains used include *P. aeruginosa* (PA01- ATCC 47085), *P. aeruginosa* (J3284-clinical isolate), *A. baumannii* (J3433 Clinical Isolate), *S. maltophilia* (J3270 Clinical Isolate), *K. pneumoniae* (ATCC BAA1706), *E. coli* (ATCC 25922), *H. influenzae* (Clinical Isolate), Methicillin Resistant *S. aureus* (ATCC 25923), Methicillin Sensitive *S. aureus* (ATCC 252), *S. pneumoniae* (D39 NCTC 7466), *B. cenocepacia* (J2315 and K56-2 both clinical isolates) and GFP fluorescent *S. aureus* (RN6390-Gfp-EryR). Bacterial cultures were reconstituted to 0.5 OD_{595}nm for confocal assays, 0.01 OD_{595}nm for flow cytometry or 2 OD_{595}nm for ovine *ex vivo* lung experiments. Colony forming units per milliliter (CFU/mL) were enumerated by plating serial dilution to 8th $\log_{10}$ dilution on broth/blood agar plates and incubation at 37 ^{o}C for 16 hours (for *S. pneumoniae* supplemented with 5% CO_2). Identification of bacterial species was confirmed through the bacterial diagnostic laboratories, New Royal Infirmary of Edinburgh, Edinburgh, UK.

Neutrophil and monocyte isolation: Cells were isolated from the peripheral blood of healthy human volunteers as previously described(*44*).

BAL Macrophage Isolation: Bronchoalveolar lavage from patients undergoing bronchoscopy was taken and macrophages were isolated and imaged in co-culture experiments.

Emission Spectra: The fluorescence emission of NBD-PMX solutions were measured in a Synergy H1 Multi-Mode Spectrophotometer (BioTek, VT, US) upon excitation at 450 nm in increasing concentrations of Dimethyl sulfoxide (DMSO) (Sigma-Aldrich).

Haemolysis Assay: See Supplementary Information.

***In vitro* bacterial labelling and confocal assessment:** 8-Well Lab-Tek II Confocal Chambers (VWR, PA, USA) were coated in fibronectin (for mammalian cell experiments) or poly-D-lysine (for bacteria) at 37 ^{o}C for 20 minutes, then washed in PBS. Bacteria were counterstained and co-incubated with NBD-PMX at the required concentrations in a single 8-well chamber. For co-culture assays, neutrophils, mononuclear cells or alveolar macrophages were seeded in each well (1 x 10^5 per well) for 20 minutes with Syto 60 (Invitrogen, CA, USA) (5 μM) and non-adherent cells aspirated prior to bacterial and NBD-PMX inoculation. For imaging in human lung tissue, lung tissue was dissected into thin sections and incubated in a 48 well plate with bacteria. To each well, 5 μM Syto 82 (Invitrogen, CA, USA) and NBD-PMX at final concentration was added, incubated for 15 minutes and without a wash step was placed on a glass slide and a 13 mm coverslip was placed over the sample and edges sealed. A laser-scanning confocal imaging system (LSM510; Carl Zeiss, Jena, Germany), incorporating an upright Axioskop FS2 microscope (63× objective) was used. 'Green' fluorescence (for NBD) was excited with a dedicated 488 nm line (detected with meta detector at 500-530 nm), Syto 82 nuclear acid dyes were excited with a dedicated 543 nm line (detected with meta detector at 570-610 nm) and Syto 60 nuclear acid dyes were excited with a dedicated 633nm line (detected with a meta detector at 660-700 nm). Analysis was performed with ImageJ (version 1.46r, National Institutes of Health, USA); the Syto channel was thresholded and the ROI generated was quantified on the NBD channel. All experiments were performed at least three times unless otherwise stated. For analyses where direct comparison of fluorescence was made, the confocal settings for the NBD channel were kept identical between experiments.

Flow Cytometry: Smartprobe (50µL) or PBS were added to 50µL of counterstained bacteria and incubated for 5 minutes at 37ºC. Samples were diluted to 500µL immediately prior to analysis using BD FACSCalibur (Becton Dickenson, San Jose, CA, USA) flow cytometer capturing 50,000 of counterstained gated events. Voltages remained constant throughout the experiment and data was collected on a logarithmic scale. Analysis was using FlowJo version 7.6.5 (TreeStar Inc., Ashland, OR) where the counterstain was gated to eliminate debris and artefact, followed by histogram analysis of the FL-1 (Smartprobe) channel. For quantification, the mean of the FL-1 channel (Smartprobe) was recorded and data presented as the mean fluorescence from independent experiments.

Murine intra-tracheal administration: See Supplementary Information.

GLP Toxicity Study: A single dose, intra-tracheal rat toxicity study was undertaken by a Covance Labarotories (Harrogate, UK) under GLP conditions and conducted in accordance with the requirements of the Animals (Scientific Procedures) Act 1986. Crl:WI(Han) strain rats (Charles River Laboratories, Margate UK) were acclimatised for 2 weeks prior to a single intratracheal dose of 100 µg NBD-PMX or PBS control. Animals were monitored daily, provided with *ad libitum* water and maintenance diet. Animals were weighed daily, and sub-groups were sacrificed at day 3 or day 15 with assessment of haematological, coagulation and clinical chemistry tests. At necroscopy animals underwent macroscopic and microscopic pathologocal assessment of organs.

Ovine model: Ewes which were destined for cull were terminally euthanized with an overdose of anaesthetic. The right pulmonary artery was identified, cannulated and perfused with 1000ml 0.9% NaCl with free drainage from the left ventricle. The trachea was intubated with an 8.0 endotracheal tube and lungs were placed in a neonatal incubator with an ambient temperature of 37ºC, humidity of 65% and ventilated using a Pressure Controlled Ventilator (Vivo PV 403, Breas Medical, Sweden). For positive control data GFP expressing *S. aureus* were instilled via a flexible catheter (1.5mm APC catheter, ERBE, GA, USA) and bronchoscopic guidance into a naive segment and subsequently imaged

with a clinically approved OEM imaging system (Cellvizio™, Mauna Kea Technologies, Paris, France) capturing images at 12 frames per second with a field of view of ~305x430 µm. Imaging was undertaken with a 1.4 mm Alveoflex™ fibre, using a 488nm laser excitation source with constant laser power between experiments. For *in situ* bacterial labelling following 1 hour of optimal ventilation, bronchoscopy (Pentax EB-1530 T3 Video Bronchoscope) was undertaken with proximal wedging of the bronchoscope at individual segments followed by instillation of 2 mL of bacteria or PBS control via a flexible catheter (1.5mm APC catheter, ERBE, GA, USA). One hour later, a separate catheter was introduced into the working channel and NBD-PMX instilled into the distal bronchopulmonary segments. Then the Alveoflex fibre was passed down the working channel and the same segment was imaged with up to 5 transbronchial passes and recorded (recorded at 12 frames per second for minimum of two minutes). Importantly, images were only captured after entry into the distal alveolar regions determined by observing characteristic alveolar structures. For BALF, the bronchoscope was wedged distally and 20 mL of 0.9% NaCl instilled and carefully withdrawn with lavage yields of 40-50%. Control segments were anatomically distinct and/or in the contralateral lung and images prior to the introduction of bacterial cultures to the lung to prevent contamination. The bronchoscope was decontaminated between each bacterial segment imaged.

***In vivo* study:** Patients with known bronchiectasis were recruited from the Regional Specialist Bronchiectasis service. All patients underwent written and informed consent and underwent pre-bronchoscopy peripheral blood sampling and x-ray imaging and Computerized Tomography (CT) imaging. Bronchoscopy was undertaken in a dedicated endoscopy suite and a flexible fibreoptic bronchoscope (Olympus BF-1T260 or Olympus BF-260) with conscious sedation using intravenous benzodiazepine and/or short acting opiate, in keeping with routine practice in our institution. Patients were monitored continuously throughout the procedure and subsequently in a clinical environment for 4 hours, following which they were discharged home. All patients were contacted at 24 hours to assess for any adverse events. For the ICU cohort, consent was obtained from a personal legal representative as patients did not have capacity. These patients were identified by the attending ICU consultant where there was suspected pneumonia, and the patient was due to undergo bronchoscopy and lavage. In ICU

all procedures were done at the point-of care and the APACHE II score(*45*) and associated Hospital Mortality Probability Score calculated. The segment for NBD-PMX administration and OEM was chosen based upon the most affected region based on CT (for bronchiectasis patients) or guided by the chest x-ray changes and endobronchial examination and targeting of the segment with the greatest degree of mucopurulence. If the changes were widespread, then the posterior segment of the right lower lobe would be targeted. For all patients the bronchoscope was navigated to an affected segment where baseline (pre-SmartProbe) imaging was undertaken using a clinically approved 488nm laser excitation source OEM imaging system (Cellvizio^{TM}, Mauna Kea Technologies, Paris, France) and 1.4 mm Alveoflex^{TM} fibre recording at 12 frames per second, through the working channel of the bronchoscope. This clinical system recorded a larger circular field of view of ~600 µm diameter. GMP manufactured NBD-PMX was instilled into the bronchopulmonary segment via a flexible catheter (1.5mm APC catheter, ERBE, GA, USA). Following removal of the flexible catheter, the Alveoflex was re-inserted into the working channel and images were recorded for up to 2 minutes. BAL was subsequently undertaken in the same segment and bacteria were enumerated and identified. Sputum culture was also obtained where possible for the bronchiectasis cohort. Patients were monitored continuously in ICU post procedure and were discharged from the study at 4 hours.

Image analysis: A bespoke image processing algorithm was developed to detect bacteria, which appear as bright speckles in OEM imaging, utilizing two commonly used image processing algorithms, namely Laplacian of Gaussian (LoG) and Difference of Gaussian (DOG) filtering(*46-48*). The algorithm was developed in the Matlab software environment (MathWorks Inc., Natick, MA) and all digital videos were transferred offline in the manufacturer's proprietary file format (.mkt) from Cellvizio^{TM} (Mauna Kea Technologies, Paris, France) to a PC workstation. Each video file was deconstructed into individual frames, with each frame being processed independently. For each frame, irrelevant background content was suppressed by subdividing the image into multiple parts, calculating the average regional pixel signal intensity, and then suppressing all pixels within the region, which were below an experimentally derived cut-off value of between 4 to 6 times the standard deviation. Each frame then underwent LoG and DoG filtering to enhance bright spots (combined filter applied); and the center of each bright spot

was localized, and the size and coordinates of its location recorded. A further criterion defined the maximum spot size so as to discard clusters of unresolvable bright/enhanced regions which could not be attributed to the detection of bacteria. Frames were considered positive if there were >80 dots per frame for *ex vivo* data. Data is presented as the proportion of frames over a video sequence containing >80 dots per frame. For *in vivo* human imaging, the field of view was larger and consequently a higher dots per frame of >160 was assigned. Furthermore, as there was a higher proportion of background noise due to increased elastin autofluorescence in aged humans, a second size criterion was applied excluding small single pixel dots to eliminate noise. As not all frames contained relevant information, due to positioning of the instrument or movement, redundant frames from the *in vivo* study were not included in the analysis. For inclusion, a target must have been present in a sequence of greater than 5 continuous frames. Frames were excluded if any of the following were present; i) absence of background fluorescence, ii) motion blur present, iii) >50% of image obscured due to fluid bubbles or iv) large airway or bronchus imaging.

Statistical Analysis: All experiments were performed at least three times unless otherwise stated and results expressed as mean ± SEM. Data was analysed by Students t-test or ANOVA, significance was determined as $p<0.05$ (GraphPad Prism version 5.01 for Windows, GraphPad Software, San Diego California USA).

Supplementary Materials

Supplementary Methods

Movie S1: GFP expressing S. aureus instilled in ovine bronchopulmonary segment and imaged with OEM.

Movie S2: Patient D1 imaged post administration of NBD-PMX (no bacterial signal seen).

Movie S3: Patient D2 imaged post administration of NBD-PMX (bacterial signal seen).

Movie S4: Patient D3 imaged post administration of NBD-PMX (no bacterial signal seen).

Movie S5: Patient D4 imaged post administration of NBD-PMX (no bacterial signal seen).

Movie S6: Patient D5 imaged post administration of NBD-PMX (bacterial signal seen).

Movie S7: Patient D6 imaged post administration of NBD-PMX (bacterial signal seen).

Movie S8: ICU patient D7 imaged post administration of NBD-PMX (bacterial signal seen).

Movie S9: ICU patient D8 imaged post administration of NBD-PMX (no bacterial signal seen).

Movie S10: ICU patient D9 imaged post administration of NBD-PMX (no bacterial signal seen).

Movie S11: ICU patient D11 imaged post administration of NBD-PMX (bacterial signal seen).

Movie S12: ICU patient D12 imaged post administration of NBD-PMX (no bacterial signal seen).

Movie S13: ICU patient D13 imaged post administration of NBD-PMX (no bacterial signal seen).

References

1. A. Y. Peleg, D. C. Hooper, Hospital-acquired infections due to gram-negative bacteria. *New England Journal of Medicine* **362**, 1804-1813 (2010).
2. C. H. Marquette, M. C. Copin, F. Wallet, R. Neviere, F. Saulnier, D. Mathieu, A. Durocher, P. Ramon, A. B. Tonnel, Diagnostic tests for pneumonia in ventilated patients: prospective evaluation of diagnostic accuracy using histology as a diagnostic gold standard. *Am J Respir Crit Care Med* **151**, 1878-1888 (1995).
3. A. Torres, M. el-Ebiary, L. Padró, J. Gonzalez, J. P. de la Bellacasa, J. Ramirez, A. Xaubet, M. Ferrer, R. Rodriguez-Roisin, Validation of different techniques for the diagnosis of ventilator-associated pneumonia. Comparison with immediate postmortem pulmonary biopsy. *Am J Respir Crit Care Med* **149**, 324-331 (1994).
4. ATS/IDSA, Guidelines for the management of adults with hospital-acquired, ventilator-associated, and healthcare-associated pneumonia. *Am J Respir Crit Care Med* **171**, 388-416 (2005).
5. A. Torres, M. El-Ebiary, Bronchoscopic BAL in the diagnosis of ventilator-associated pneumonia. *Chest* **117**, 198-202 (2000).
6. R. P. Baughman, Protected-specimen brush technique in the diagnosis of ventilator-associated pneumonia. *Chest* **117**, 203S-206S (2000).
7. A. Rea-Neto, N. C. Youssef, F. Tuche, F. Brunkhorst, V. M. Ranieri, K. Reinhart, Y. Sakr, Diagnosis of ventilator-associated pneumonia: a systematic review of the literature. *Crit Care* **12**, R56 (2008).
8. V. S. Baselski, R. G. Wunderink, Bronchoscopic diagnosis of pneumonia. *Clinical microbiology reviews* **7**, 533-558 (1994).
9. A. Torres, A. Martos, J. Puig De La Bellacasa, M. Ferrer, M. El-Ebiary, J. González, A. Gené, R. Rodríguez-Roisin, Specificity of endotracheal aspiration, protected specimen brush, and bronchoalveolar lavage in mechanically ventilated patients. *American Review of Respiratory Disease* **147**, 952-952 (1993).

10. E. Prats, J. Dorca, M. Pujol, L. Garcia, B. Barreiro, R. Verdaguer, F. Gudiol, F. Manresa, Effects of antibiotics on protected specimen brush sampling in ventilator-associated pneumonia. *European Respiratory Journal* **19**, 944-951 (2002).

11. G. U. Meduri, R. C. Reddy, T. Stanley, F. El-Zeky, Pneumonia in acute respiratory distress syndrome. A prospective evaluation of bilateral bronchoscopic sampling. *Am J Respir Crit Care Med* **158**, 870-875 (1998).

12. G. U. Meduri, J. Chastre, The standardization of bronchoscopic techniques for ventilator-associated pneumonia. *CHEST Journal* **102**, 557S-564S (1992).

13. S. Bousbia, L. Papazian, P. Saux, J. M. Forel, J.-P. Auffray, C. Martin, D. Raoult, B. La Scola, Repertoire of Intensive Care Unit Pneumonia Microbiota. *PLoS ONE* **7**, e32486 (2012).

14. D. R. Storm, K. S. Rosenthal, P. E. Swanson, Polymyxin and Related Peptide Antibiotics. *Annual Review of Biochemistry* **46**, 723-763 (1977).

15. M. Shaheen, J. Li, Avena C. Ross, John C. Vederas, Susan E. Jensen, Paenibacillus polymyxa PKB1 Produces Variants of Polymyxin B-Type Antibiotics. *Chemistry & biology* **18**, 1640-1648 (2011).

16. P. Pristovsek, J. Kidric, Solution structure of polymyxins B and E and effect of binding to lipopolysaccharide: an NMR and molecular modeling study. *Journal of medicinal chemistry* **42**, 4604-4613 (1999).

17. T. Velkov, P. E. Thompson, R. L. Nation, J. Li, Structure−Activity Relationships of Polymyxin Antibiotics. *Journal of medicinal chemistry* **53**, 1898-1916 (2010).

18. E. Mahenthiralingam, T. Coenye, J. W. Chung, D. P. Speert, J. R. W. Govan, P. Taylor, P. Vandamme, Diagnostically and experimentally useful panel of strains from the Burkholderia cepacia complex. *Journal of Clinical Microbiology* **38**, 910-913 (2000).

19. S. A. Loutet, F. Di Lorenzo, C. Clarke, A. Molinaro, M. A. Valvano, Transcriptional responses of Burkholderia cenocepacia to polymyxin B in isogenic strains with diverse polymyxin B resistance phenotypes. *BMC genomics* **12**, 472 (2011).

20. J. D. Chalmers, P. Goeminne, S. Aliberti, M. J. McDonnell, S. Lonni, J. Davidson, L. Poppelwell, W. Salih, A. Pesci, L. J. Dupont, The bronchiectasis severity index. An international derivation and validation study. *Am J Respir Crit Care Med* **189**, 576-585 (2014).

21. U. Schwab, L. H. Abdullah, O. S. Perlmutt, D. Albert, C. W. Davis, R. R. Arnold, J. R. Yankaskas, P. Gilligan, H. Neubauer, S. H. Randell, Localization of Burkholderia cepacia complex bacteria in cystic fibrosis lungs and interactions with Pseudomonas aeruginosa in hypoxic mucus. *Infection and immunity* **82**, 4729-4745 (2014).

22. B. Mills, M. Bradley, K. Dhaliwal, Optical imaging of bacterial infections. *Clinical and Translational Imaging* **4**, 163-174 (2016).

23. F. J. Hernandez, L. Huang, M. E. Olson, K. M. Powers, L. I. Hernandez, D. K. Meyerholz, D. R. Thedens, M. A. Behlke, A. R. Horswill, J. O. McNamara II, Noninvasive imaging of Staphylococcus aureus infections with a nuclease-activated probe. *Nat Med* **20**, 301-306 (2014).

24. X. Ning, S. Lee, Z. Wang, D. Kim, B. Stubblefield, E. Gilbert, N. Murthy, Maltodextrin-based imaging probes detect bacteria in vivo with high sensitivity and specificity. *Nat Mater* **10**, 602-607 (2011).

25. P. Panizzi, M. Nahrendorf, J. L. Figueiredo, J. Panizzi, B. Marinelli, Y. Iwamoto, E. Keliher, A. A. Maddur, P. Waterman, H. K. Kroh, F. Leuschner, E. Aikawa, F. K. Swirski, M. J. Pittet, T. M. Hackeng, P. Fuentes-Prior, O. Schneewind, P. E. Bock, R. Weissleder, In vivo detection of Staphylococcus aureus endocarditis by targeting pathogen-specific prothrombin activation. *Nat Med* **17**, 1142-1146 (2011).

26. M. van Oosten, T. Schäfer, J. A. Gazendam, K. Ohlsen, E. Tsompanidou, M. C. de Goffau, H. J. Harmsen, L. M. Crane, E. Lim, K. P. Francis, Real-time in vivo imaging of invasive-and biomaterial-associated bacterial infections using fluorescently labelled vancomycin. *Nature communications* **4**, (2013).

27. L. Thiberville, M. Salaun, S. Lachkar, S. Dominique, S. Moreno-Swirc, C. Vever-Bizet, G. Bourg-Heckly, Human in vivo fluorescence microimaging of the alveolar ducts and sacs during bronchoscopy. *The European respiratory journal* **33**, 974-985 (2009).

28. M. E. Evans, D. J. Feola, R. P. Rapp, Polymyxin B sulfate and colistin: old antibiotics for emerging multiresistant gram-negative bacteria. *Ann Pharmacother* **33**, 960-967 (1999).

29. A. S. Levin, A. A. Barone, J. Penço, M. V. Santos, I. S. Marinho, E. A. G. Arruda, E. I. Manrique, S. F. Costa, Intravenous Colistin as Therapy for Nosocomial Infections Caused by Multidrug-Resistant Pseudomonas aeruginosa and Acinetobacter baumannii. *Clinical Infectious Diseases* **28**, 1008-1011 (1999).

30. A. A. Peterson, R. E. Hancock, E. J. McGroarty, Binding of polycationic antibiotics and polyamines to lipopolysaccharides of Pseudomonas aeruginosa. *J Bacteriol* **164**, 1256-1261 (1985).

31. A. Cannatelli, M. M. D'Andrea, T. Giani, V. Di Pilato, F. Arena, S. Ambretti, P. Gaibani, G. M. Rossolini, In Vivo Emergence of Colistin Resistance in Klebsiella pneumoniae Producing KPC-Type Carbapenemases Mediated by Insertional Inactivation of the PhoQ/PhoP mgrB Regulator. *Antimicrobial Agents and Chemotherapy* **57**, 5521-5526 (2013).

32. Y.-Y. Liu, Y. Wang, T. R. Walsh, L.-X. Yi, R. Zhang, J. Spencer, Y. Doi, G. Tian, B. Dong, X. Huang, L.-F. Yu, D. Gu, H. Ren, X. Chen, L. Lv, D. He, H. Zhou, Z. Liang, J.-H. Liu, J. Shen, Emergence of plasmid-mediated colistin resistance mechanism MCR-1 in animals and human beings in China: a microbiological and molecular biological study. *The Lancet Infectious Diseases* **16**, 161-168 (2016).

33. J. Garnacho-Montero, C. Ortiz-Leyba, F. J. Jiménez-Jiménez, A. E. Barrero-Almodóvar, J. L. García-Garmendia, M. Bernabeu-Wittell, S. L. Gallego-Lara, J. Madrazo-Osuna, Treatment of Multidrug-Resistant Acinetobacter baumannii Ventilator-Associated Pneumonia (VAP) with Intravenous Colistin: A Comparison with Imipenem-Susceptible VAP. *Clinical Infectious Diseases* **36**, 1111-1118 (2003).

34. V. M. Manikal, D. Landman, G. Saurina, E. Oydna, H. Lal, J. Quale, Endemic Carbapenem-Resistant Acinetobacter Species in Brooklyn, New York: Citywide Prevalence, Interinstitutional Spread, and Relation to Antibiotic Usage. *Clinical Infectious Diseases* **31**, 101-106 (2000).

35. D. Yong, M. A. Toleman, C. G. Giske, H. S. Cho, K. Sundman, K. Lee, T. R. Walsh, Characterization of a new metallo-beta-lactamase gene, bla(NDM-1), and a novel erythromycin esterase gene carried on a unique genetic structure in Klebsiella pneumoniae sequence type 14 from India. *Antimicrob Agents Chemother* **53**, 5046-5054 (2009).

36. K. K. Kumarasamy, M. A. Toleman, T. R. Walsh, J. Bagaria, F. Butt, R. Balakrishnan, U. Chaudhary, M. Doumith, C. G. Giske, S. Irfan, P. Krishnan, A. V. Kumar, S. Maharjan, S. Mushtaq, T. Noorie, D. L. Paterson, A. Pearson, C. Perry, R. Pike, B. Rao, U. Ray, J. B. Sarma, M. Sharma, E. Sheridan, M. A. Thirunarayan, J. Turton, S. Upadhyay, M. Warner, W. Welfare, D. M. Livermore, N. Woodford, Emergence of a new antibiotic resistance mechanism in India, Pakistan, and the UK: a molecular, biological, and epidemiological study. *The Lancet. Infectious diseases* **10**, 597-602 (2010).

37. P. M. Bossuyt, J. B. Reitsma, D. E. Bruns, C. A. Gatsonis, P. P. Glasziou, L. Irwig, J. G. Lijmer, D. Moher, D. Rennie, H. C. W. de Vet, H. Y. Kressel, N. Rifai, R. M. Golub, D. G. Altman, L. Hooft, D. A. Korevaar, J. F. Cohen, STARD 2015: an updated list of essential items for reporting diagnostic accuracy studies. *BMJ : British Medical Journal* **351**, (2015).

38. J. Stone, H. Wood, K. Harrington, T. Birks, Low index contrast imaging fibers. *Optics Letters* **42**, 1484-1487 (2017).

39. N. Krstajić, A. R. Akram, T. R. Choudhary, N. McDonald, M. G. Tanner, E. Pedretti, P. A. Dalgarno, E. Scholefield, J. M. Girkin, A. Moore, Two-color widefield fluorescence microendoscopy enables multiplexed molecular imaging in the alveolar space of human lung tissue. *Journal of biomedical optics* **21**, 046009-046009 (2016).

40. M. Aguilar-Guisado, J. Givalda, P. Ussetti, A. Ramos, P. Morales, M. Blanes, G. Bou, J. d. Torre-Cisneros, A. Roman, J. Borro, Pneumonia after lung transplantation in the RESITRA Cohort: a multicenter prospective study. *American Journal of Transplantation* **7**, 1989-1996 (2007).

41. J. Chastre, J.-Y. Fagon, Ventilator-associated Pneumonia. *Am J Respir Crit Care Med* **165**, 867-903 (2002).

42. A. Combes, C. Figliolini, J.-L. Trouillet, N. Kassis, M. Wolff, C. Gibert, J. Chastre, Incidence and outcome of polymicrobial ventilator-associated pneumonia. *Chest* **121**, 1618-1623 (2002).

43. A. R. Akram, N. Avlonitis, A. Lilienkampf, A. M. Perez-Lopez, N. McDonald, S. V. Chankeshwara, E. Scholefield, C. Haslett, M. Bradley, K. Dhaliwal, A Labelled-Ubiquicidin Antimicrobial Peptide for Immediate In Situ Optical Detection of Live Bacteria in Human Alveolar Lung Tissue. *Chem. Sci.* **6**, 6971-6979 (2015).

44. C. Haslett, L. A. Guthrie, M. M. Kopaniak, R. B. Johnston, Jr., P. M. Henson, Modulation of multiple neutrophil functions by preparative methods or trace concentrations of bacterial lipopolysaccharide. *Am J Pathol* **119**, 101-110 (1985).

45. W. A. Knaus, E. A. Draper, D. P. Wagner, J. E. Zimmerman, APACHE II: a severity of disease classification system. *Critical care medicine* **13**, 818-829 (1985).

46. H. Kong, H. C. Akakin, S. E. Sarma, A generalized Laplacian of Gaussian filter for blob detection and its applications. *IEEE T. Cybernetics* **43**, 1719-1733 (2013).

47. T. Lindeberg, Feature detection with automatic scale selection. *International journal of computer vision* **30**, 79-116 (1998).

48. A. Raj, P. Van Den Bogaard, S. A. Rifkin, A. Van Oudenaarden, S. Tyagi, Imaging individual mRNA molecules using multiple singly labeled probes. *Nature methods* **5**, 877-879 (2008).

49. M. Ternon, J. J. Díaz-Mochón, A. Belsom, M. Bradley, Dendrimers and combinatorial chemistry—tools for fluorescent enhancement in protease assays. *Tetrahedron* **60**, 8721-8728 (2004).

Acknowledgements: This research was supported by the National Institute for Health Research (NIHR) BRC GMP Unit at Guy's and St Thomas' NHS Foundation Trust and NIHR Biomedical Research Centre based at Guy's and St Thomas' NHS Foundation Trust and King's College London. The views expressed are those of the author(s) and not necessarily those of the NHS, the NIHR or the Department of Health. **Funding:** We would like to thank the Wellcome Trust & Department of Health Healthcare Innovation Challenge Fund (HICF-0510-069) for supporting the staff involved in this study and the Proteus Engineering and Physical Sciences Research Council Interdisciplinary Research Collaboration (EP/K03197X/1). A**uthor Contributions:** SVC, AMF, TA, NA, MV, and MB performed chemical design, synthesis and characterisation. ARA, NM, ES, BM, CH, MB and KD designed and performed the in vitro biological assays. ES and KD designed and performed the murine work. ARA, NM, TC, DSC, ES and KD designed, set-up and performed the *ex vivo* ovine lung experiments. ARA, TC, AM, ATH, AMS, TW, CH and KD designed and undertook the *in vivo* study. ARA, NM and KD undertook data analysis. NH and JG provided cells from BALF and clinical isolates of bacterial strains and microbiology guidance respectively. CG designed the image analysis algorithm with input from ARA, NM and KD. CH, MB, TW and KD conceived and supervised the project. ARA and KD wrote the manuscript. All authors approved the manuscript. **Competing Interests:** CH, MB and KD are founder directors and have a shareholding in Edinburgh Molecular Imaging Ltd. KD has received travel and attendance fees from Mauna Kea Technologies as a consultant for an advisory board. ARA, TC, NM and KD have received travel fees for attendance at educational conferences supported by an unrestricted educational grant from Mauna Kea Technologies.

Figures 1-5 with legends below.

Supplemental information contained within a single file.

Movies 1-13 uploaded separately.

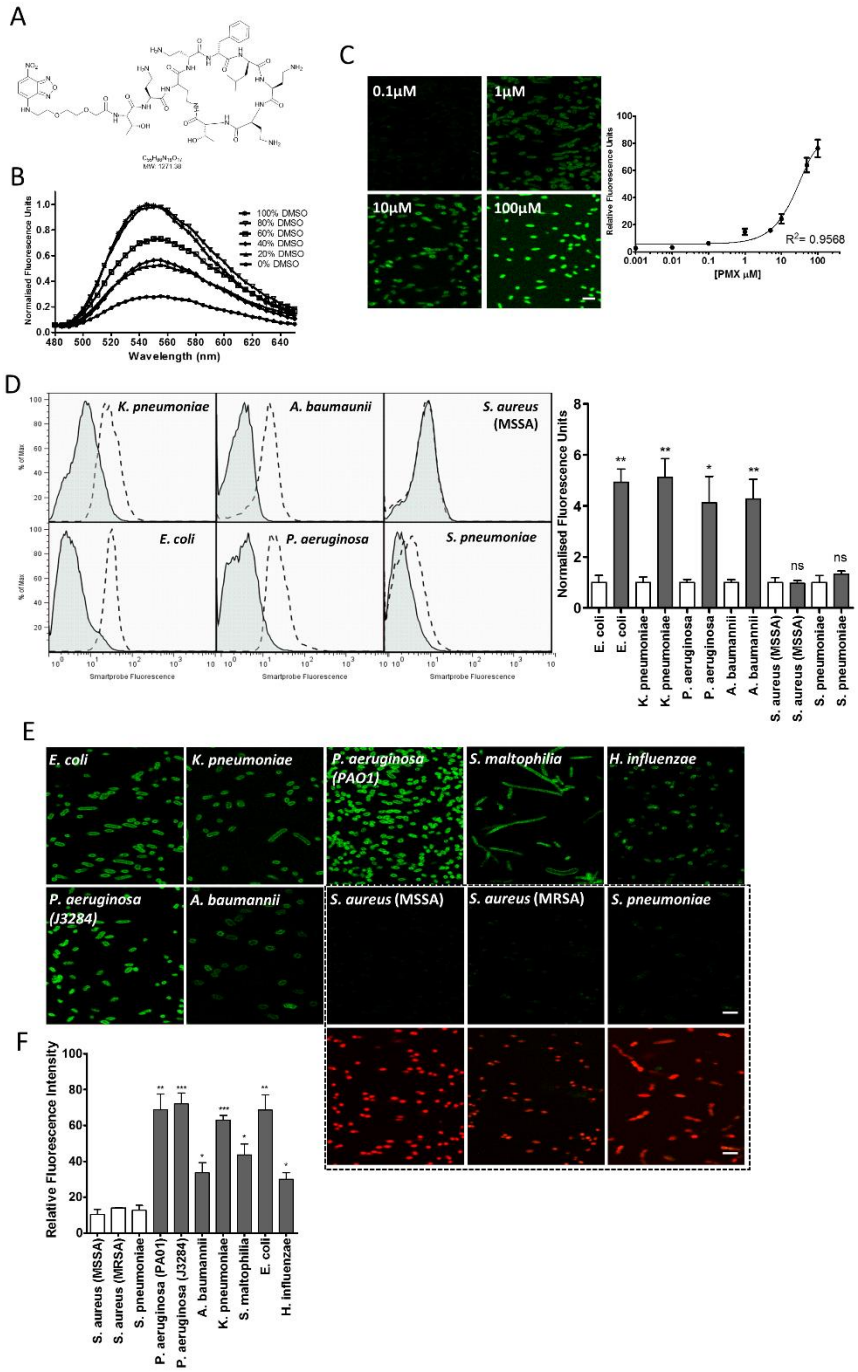

Figure 1: NBD-PMX labels gram-negative bacteria in a concentration dependent manner, with fluorescence amplification in hydrophobic environments. A) Structure of NBD-PMX; B) Fluorescence increase in increasing concentrations of Dimethyl sulfoxide (DMSO) (NBD-PMX at 5µM), n=3. C) Fluorescence quantification of *P. aeruginosa* imaged on a benchtop confocal microscope in the continued presence of increasing concentrations of NBD-PMX, demonstrating a concentration dependent fluorescent signal. Images show representative images at denoted concentration of NBD-PMX, scale bar represents 5µm. Each point on graph represents the mean (+/- SEM) of three independent experiments where at least three fields of view were quantified with a single site non-linear fit of data. D) Representative flow histograms for unstained bacteria (grey histograms) or NBD-PMX stained bacteria (5µM) (dotted line) demonstrating a greater fluorescence intensity increase for gram-negative than gram-positive bacteria. Graph shows quantification of flow cytometry data for unstained bacteria (white bars, normalized) and NBD-PMX (grey bars) demonstrating a significant increase in fluorescence for gram-negative bacteria, but no significant increase for gram positive bacteria. Bars represent means (+/- SEM) from three independent experiments, analysis is by students t-test, ns-not significant, *=p<0.05, **=p<0.01. E) Bacterial panel with NBD-PMX 1µM (green) and counterstain with Syto-82 (red). Gram-positive bacteria (bounded by box) display minimal/no labelling compared and are shown with their counterstain to demonstrate correct focal plane, scale bar represents 5µm. F) Quantification of bacterial panel with NBD-PMX (1µM) with gram-positive bacteria (white bars) and gram-negative (black bars), showing high intensity selective labelling of gram-negative bacteria compared with gram-positive. All gram-negatives showed a statistically significant increase over all gram-positives, bars show mean fluorescence (+/- SEM) from three independent experiments, where at least three fields of view were assessed. Analysis by Students t-test, *=p<0.05, **= p<0.01, ***=p<0.001.

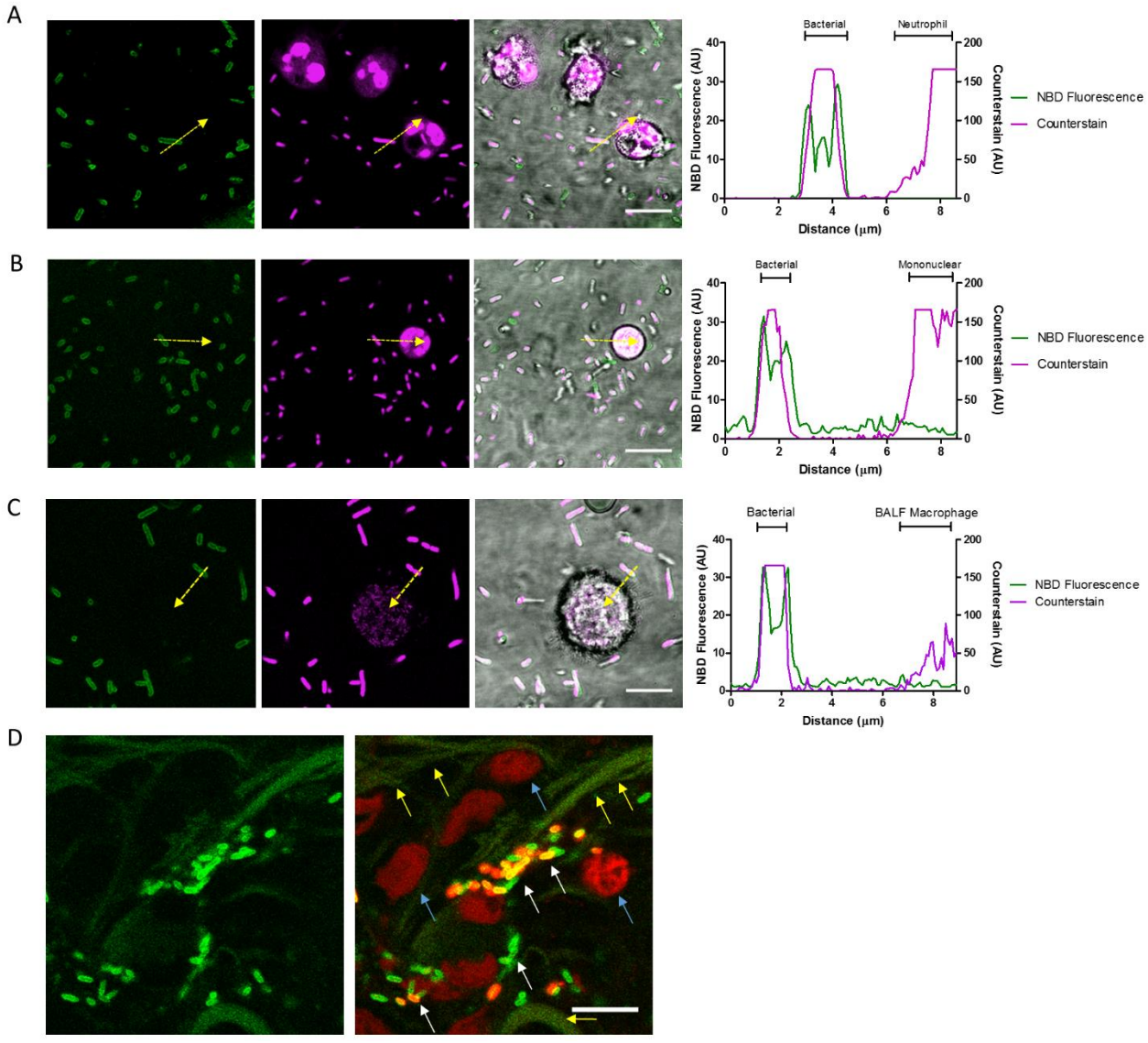

Figure 2: NBD-PMX demonstrated selectivity for bacteria over mammalian cells. Co-culture experiments of freshly isolated human neutrophils (A), freshly isolated human mononuclear cells (B) and human alveolar macrophages retrieved on bronchoalveolar lavage (C) with *P. aeruginosa* imaged in the continued presence of with NBD-PMX (5μM). Green panels demonstrate NBD fluorescence, middle panels demonstrate nuclear counterstain (Syto-60) and merge images shown on right. Plot profiles corresponding to yellow arrows shown on right with labelling of bacterial but not mammalian cell membranes. D) Confocal image of human lung tissue co-cultured with bacteria and imaged following labelling with NBD-PMX (5μM). 2 panels; left panel shows NBD and autofluorescence with excitation at 488nm and right panel shows merge with counterstain. White arrows indicate bacterial labelling, blue arrows demonstrate epithelial cells and yellow arrows demonstrate elastin autofluorescence. All experiments n=3, representative images shown, Scale bar represents 10μm.

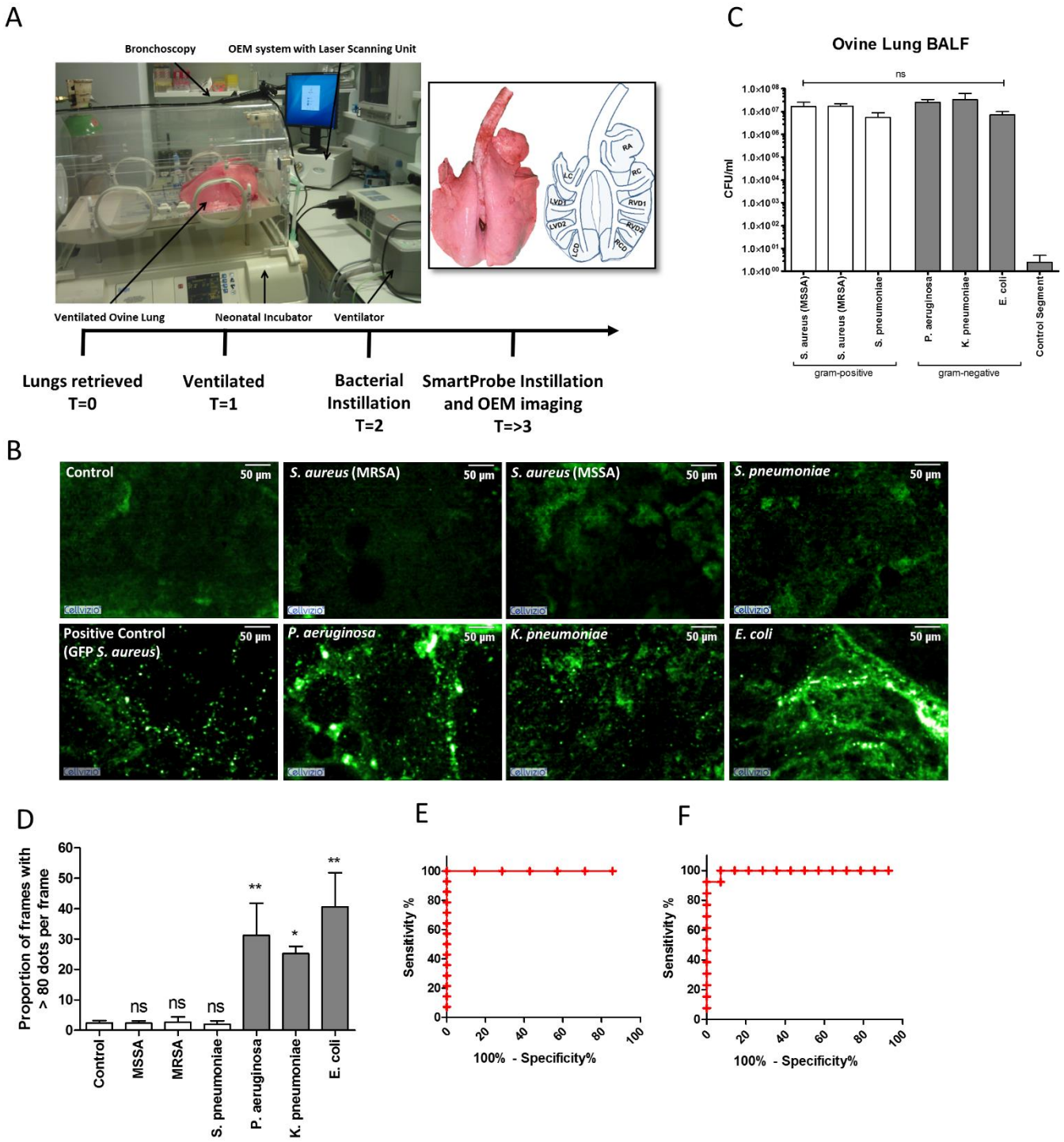

Figure 3: NBD-PMX labelled gram-negative, but not gram-positive bacteria *in situ* in *ex vivo* ovine lungs. A) Experimental set-up. Image demonstrating the anatomically distinct pulmonary segments of the ovine lung and timeline outlining the experimental protocol of retrieval, ventilation, bacterial instillation and NBD-PMX instillation and OEM imaging. B) Representative OEM images of no bacterial signal in the control or gram-positive bacteria segments (top panels), but a punctate bacterial fluorescent signal in the positive control (GFP *S. aureus*) and gram-negative segments. C) Lavage was enumerated for bacterial counts. Bacterial segments revealed no significant differences in bacterial counts, n=4 for all bacteria except *S. pneumoniae* where n=3, analysis by one-way ANOVA, ns=not significant. D) Analysis of entire videos for control segments (n=7), MSSA (n=5), MRSA (n=4), *S. pneumoniae* (n=4), *P. aeruginosa* (n=4), *K. pneumoniae* (n=5) and *E.coli* segments (n=5) demonstrating a significantly higher proportion of frames with >80 dots per frame for the gram-negative (grey bars) but not the gram-positive segments (white bars) when compared to control, bars represent mean (+/- SEM), *=p<0.05, **=p<0.01, ns=not significant, Students t-test. Receiver operator characteristics of image analysis videos; E) For control (n=7) or all gram-negative videos (n=14) the area under the curve was 1.0 (95% Confidence intervals (95%CI) 1.0-1.0), p=0.0002592. F) For gram-negative segments (n=14) compared to gram-positive segments (n=13) the AUC was 0.9945 (95%CI 0.9768-1.012), p<0.001.

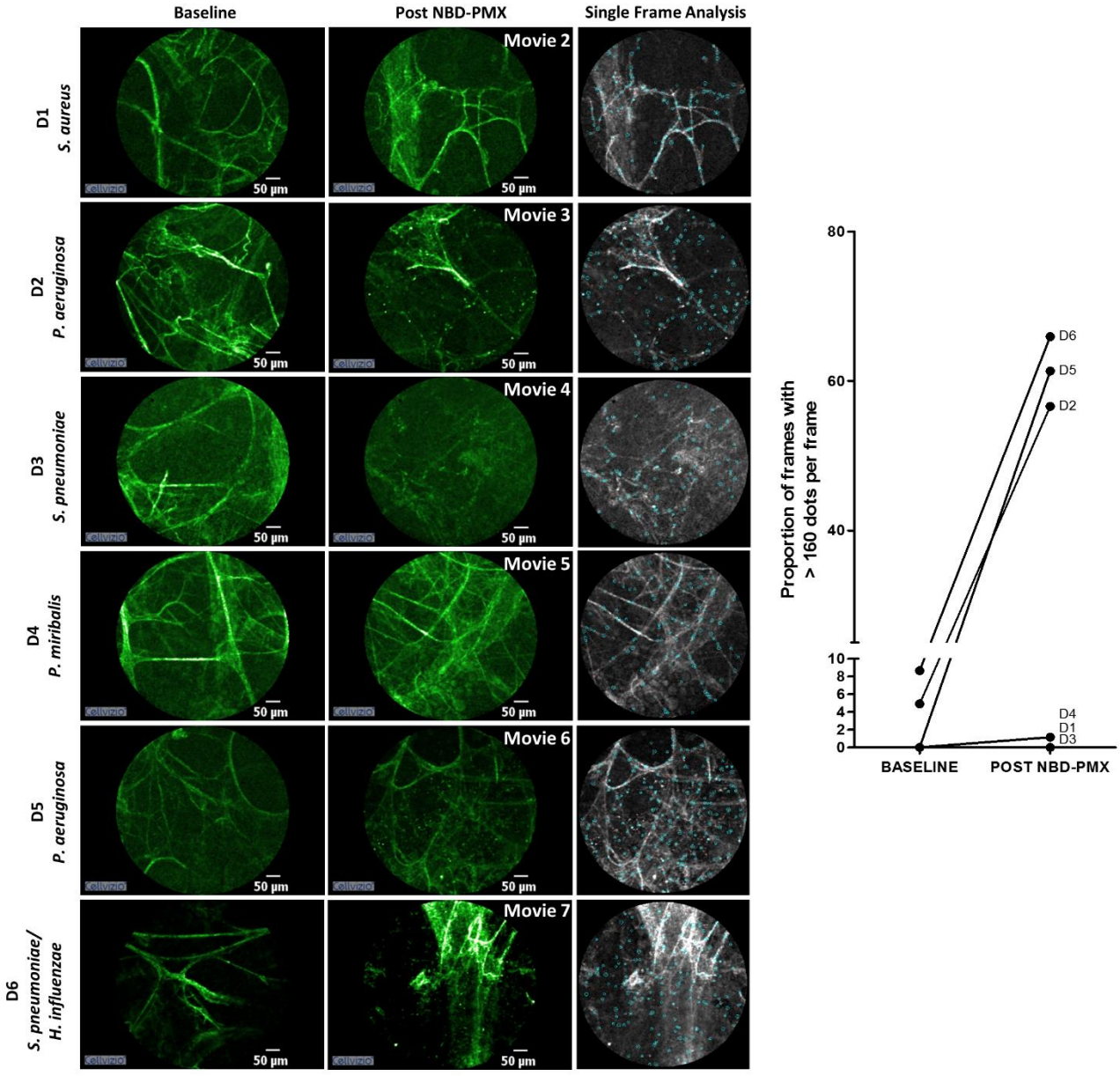

Figure 4: NBD-PMX labels gram-negative bacteria *in vivo* in humans when administered endobronchially and imaged with OEM. Representative alveolar images of baseline imaging (left) and post administration of NBD-PMX in six patients. D2, D5 and D6 demonstrated positive bacterial signal post NBD-PMX administration with dots detected in representative frame, defined by >10% frames with >160 punctate dots per frame. Graph demonstrates image analysis of individual frames from baseline imaging and post NBD-PMX demonstrating a higher proportion of frames with >160 dots per frame. Mean number of frames per video analysis was 443 frames, data shown as proportion of frames with >160 dots detected per frame.

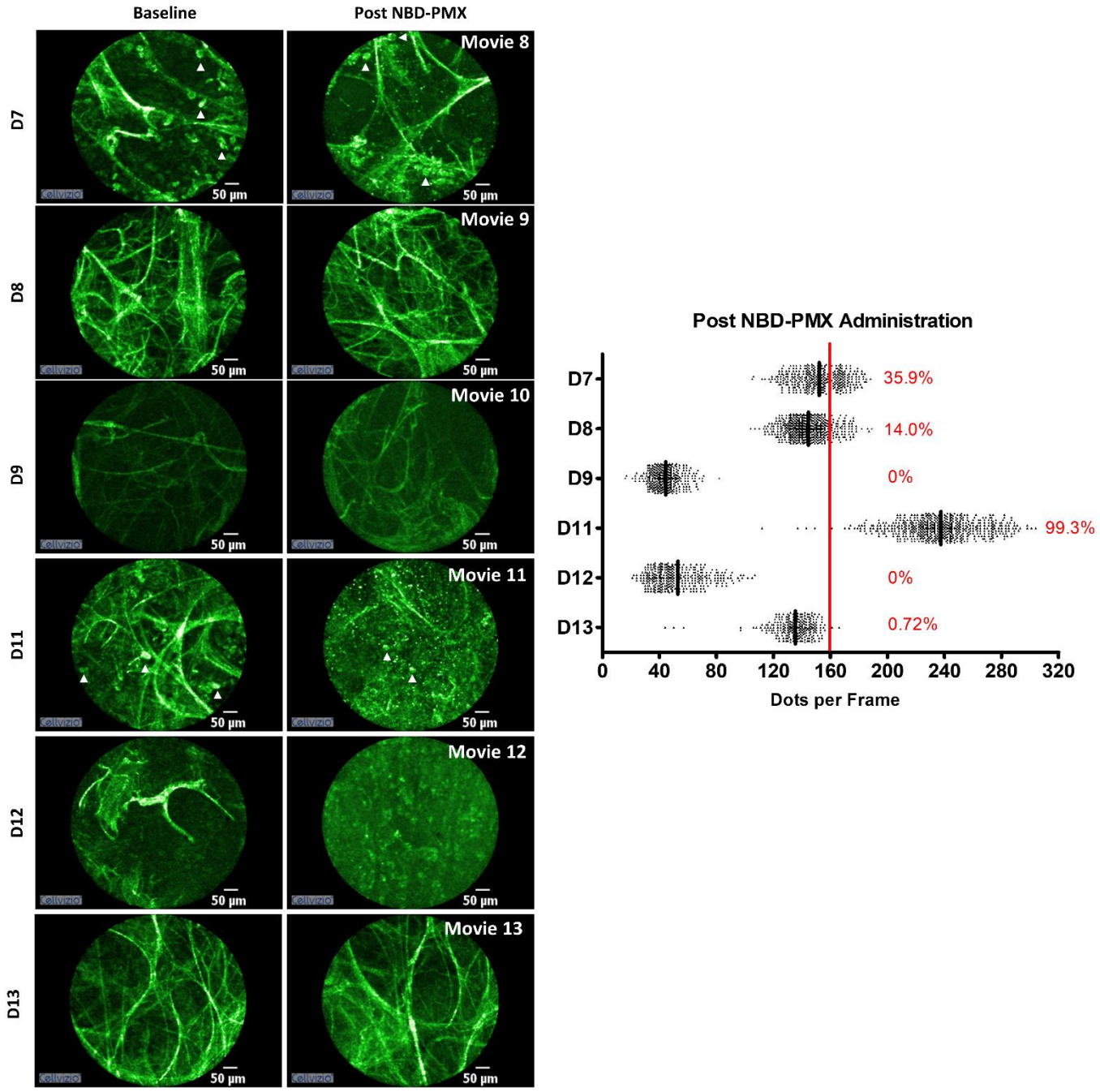

Figure 5: NBD-PMX administration and imaging in six ventilated patients in ICU. Representative alveolar images of baseline imaging (left) and post administration of NBD-PMX in six patients where pneumonia was suspected. D7 and D11 demonstrates cellular infiltrate (cells shown by white arrows) and presence of alveolar punctate signal consistent with bacterial presence. D8 and D13 demonstrates condensed elastin consistent with atelectasis, and both D9 and D12 demonstrate absence of alveolar bacterial signal. D12 demonstrates absence of alveolar structure consistent with the development of an abscess. Graph demonstrates the frame-by-frame analysis of each video sequence post NBD-PMX administration. Each point represents a single frame analysis and line represents the mean, with the % above the threashold of 160 dots per frame shown on right in red.

Immediate *In Situ* Identification of Gram-negative Bacteria in Human Lungs Using a Topical Fluorescent Peptide Targeted Against Lipid A

Ahsan R Akram, Sunay V Chankeshwara, Emma Scholefield, Tashfeen Aslam, Neil McDonald, Alicia Megia-Fernandez, Adam Marshall, Beth Mills, Nicolaos Avlonitis, Marc Vendrell, Thomas H Craven, Annya M Smyth, David S Collie, Calum Gray, Nik Hirani, Adam T Hill, John R Govan, Timothy Walsh, Christopher Haslett, Mark Bradley & Kevin Dhaliwal.

Supplementary Information

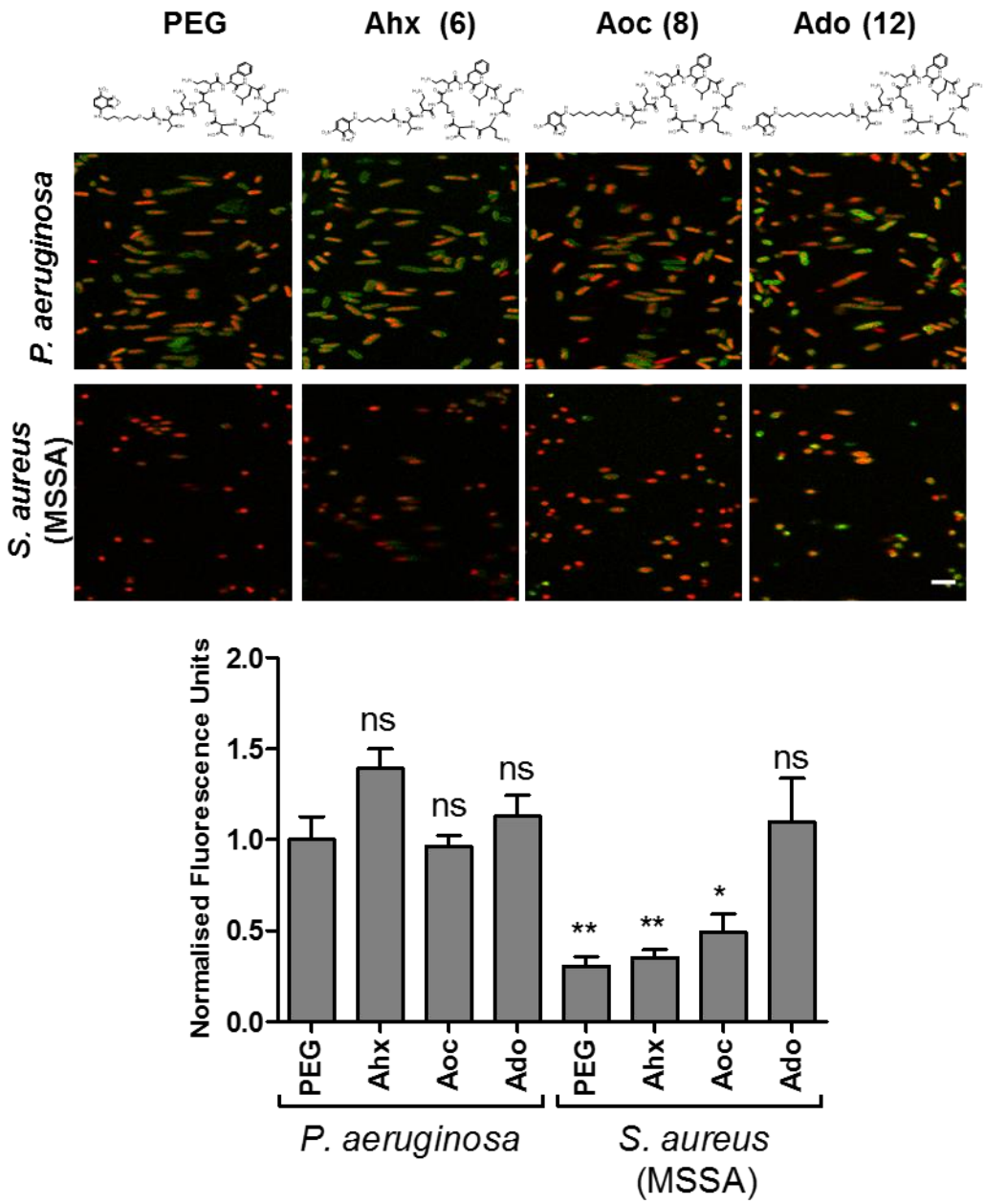

Figure S1: Progressive lengthening of the linker leads to loss of gram-selectivity. NBD-PMX constructs with Amino-3,6-dioxaoctanoic PEG2 (PEG), Aminohexanoic (Ahx) (6), Aminooctanoic (Aoc) (8) and Aminododecanoic (12) (all at 1µM) demonstrating similar fluorescence (green in panels) intensities for *P. aeruginosa* but increasing fluorescence for *Methicillin sensitive S. aureus (*MSSA) with representative merged images (with Syto-82 counterstain in red) (scale bar 5µm). Lower graph shows quantification of data and demonstrates no significant fluorescence for *P. aeruginosa* with the different constructs, but progressively increased fluorescence signal with MSSA. All data normalised and analyses compared to NBD-PMX with PEG on *P. aeruginosa*. Bars represent mean (+/- SEM), n=3, ns=not significant, *=p<0.05, **=p<0.01.

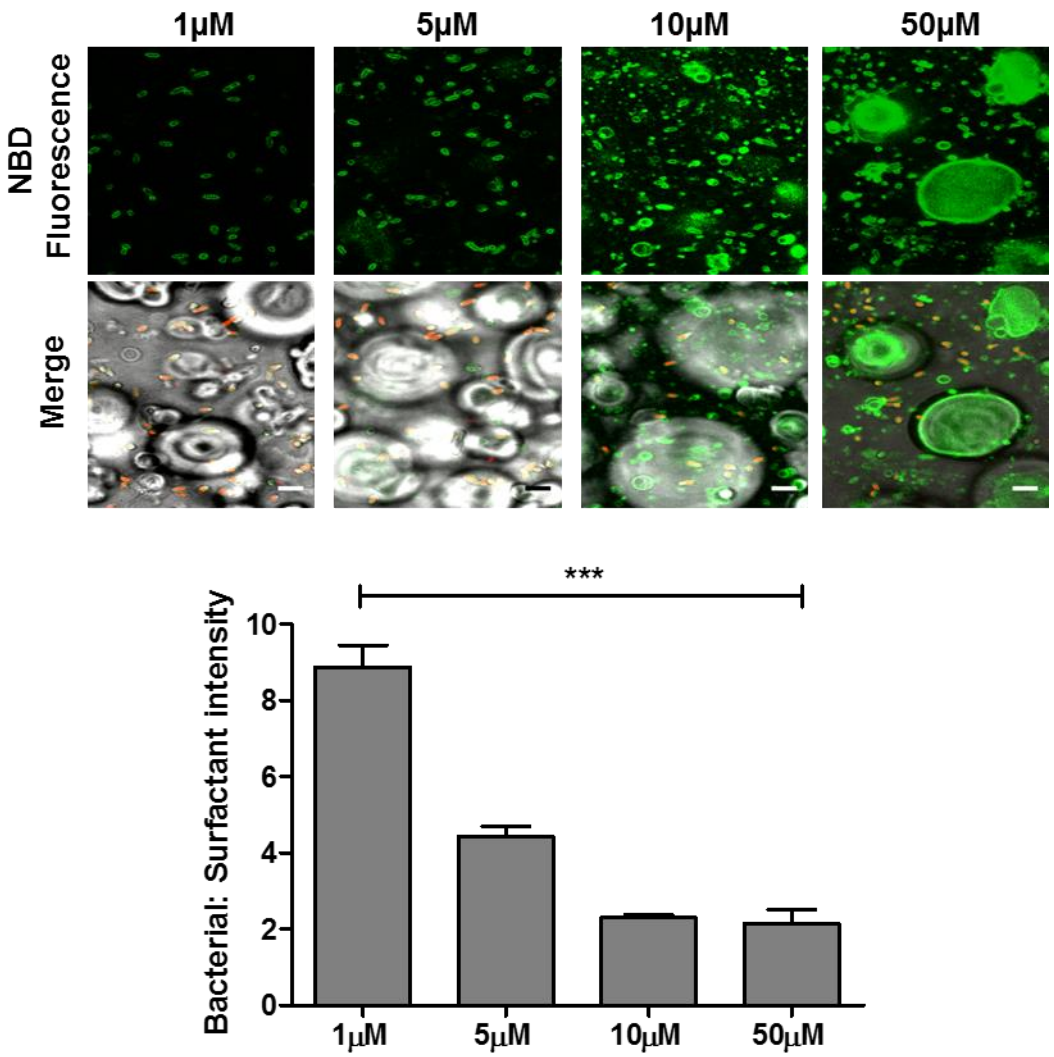

Figure S2: NBD-PMX has improved signal-to-noise at lower concentrations in the presence of pulmonary surfactant. NBD-PMX displayed increasing surfactant labelling at higher concentrations. Upper panels show fluorescence and brightfield merged images Lower graph displays quantification of bacterial fluorescence to surfactant fluorescence as a ratio. At all concentrations the fluorescence of bacteria remain higher than surfactant. Bars represent mean (+/-SEM), n=3, analysis by one way ANOVA, ***=p<0.001, scale bar represents 5µm.

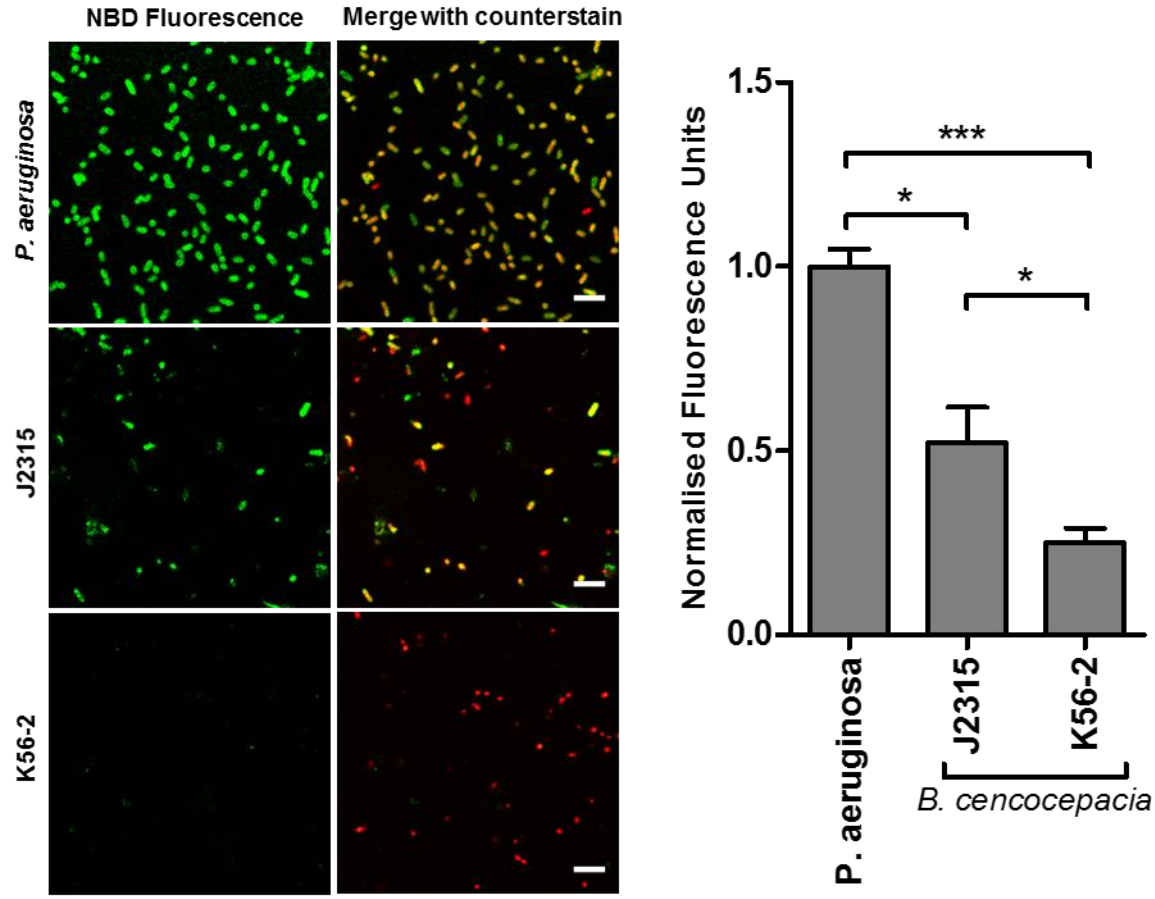

Figure S3: NBD-PMX binding with polymyxin resistant strains of *B. cenocepacia* is reduced compared to *P. aeruginosa*. Representative images (left) and quantification of fluorescence (right) of two forms of B. *cenocepacia*, with either depleted rough LPS (J2315) or smooth LPS but a mutated lipid A component (K56-2) LPS, and compared to *P. aeruginosa*. Data demonstrated there was a significant reduction in fluorescence with both strains compared to *P. aeruginosa* and a lower fluorescence intensity with K56-2 variant when compared to the J2315, bars represent mean (+/- SEM), n=4, *=p<0.05, ***=p<0.001, scale bar represents 5µm.

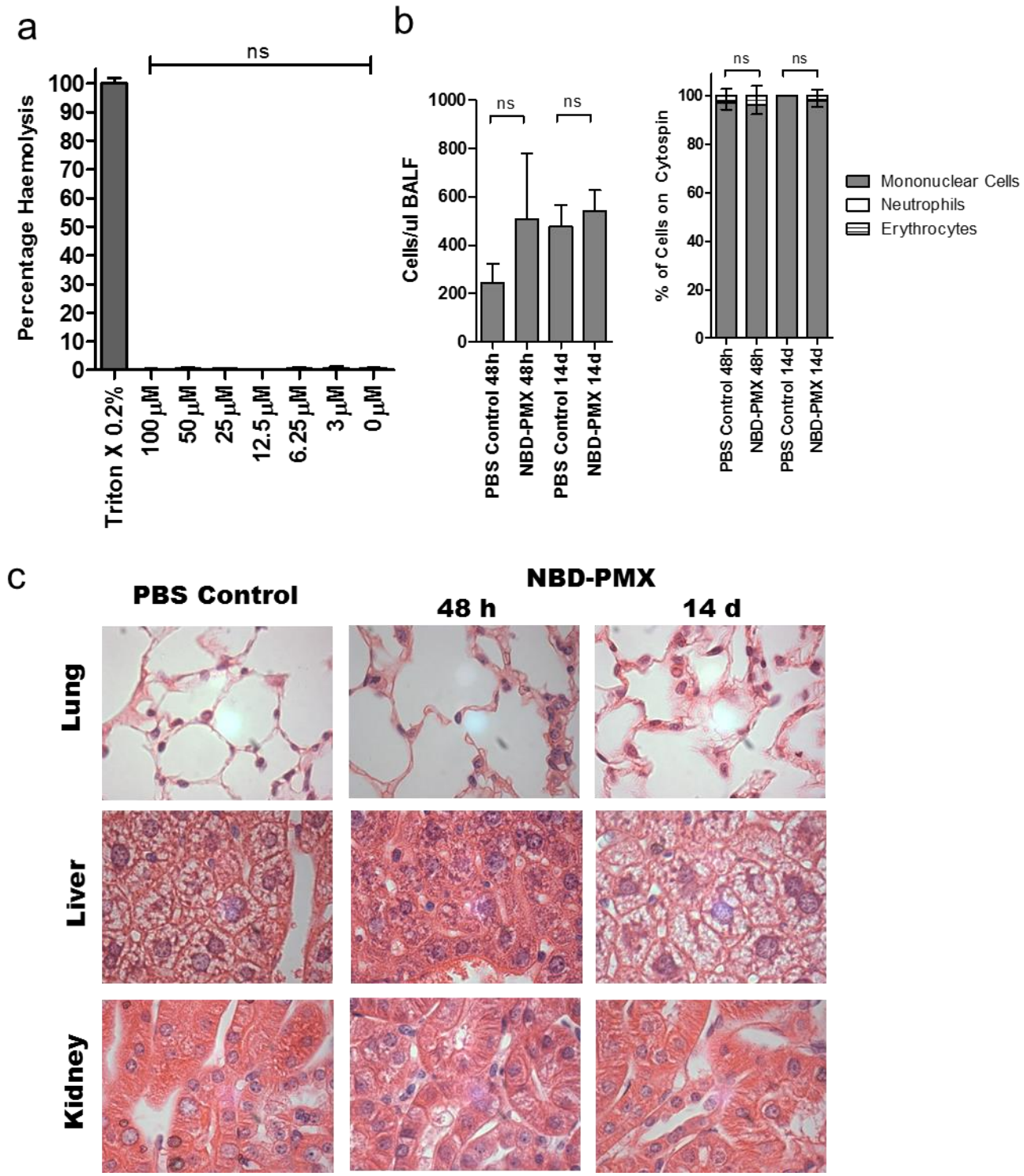

Figure S4: NBD-PMX demonstrated no cell membrane toxicity and no *in vivo* toxicity after intratracheal instillation in mice. A) No red blood cell haemolysis observed for NBD-PMX concentrations up to 100µM, n=3, bars represent mean (+/-SEM) of three independent procedures performed in duplicate. Positive control was 0.2% Triton-X and values corrected to represent 100% haemolysis for Triton-X. Statistical analysis by ANOVA., ns=not significant. B) BALF at 48 hours following intratracheal instillation of 100 micrograms of NBD-PMX (vs vehicle PBS control) demonstrated no increase in cells and no significant increase in neutrophil counts, bars represent mean (+/-SD), n=3. C) Representative histology of animals at 48 hours (x100) demonstrated no changes to microscopic architecture in lung, liver or kidney tissue.

	Control (Male)			NBD-PMX (Male)				Control (Female)			NBD-PMX (Female)			
Day (post dosing)	**Mean weight (g)**	**SD**	**n**	**Mean weight (g)**	**SD**	**n**		**Mean weight (g)**	**SD**	**n**	**Mean weight (g)**	**SD**	**n**	
1	140.2	9.71	14	140.4	10.93	15	ns	113.4	10.49	15	113.3	10.46	15	ns
2	144.8	9.5	15	146	13.96	15	ns	116.4	9.81	15	115.9	11.14	15	ns
3	152.8	13.68	5	163	11.69	5	ns	128.2	8.51	5	123.3	14.67	5	ns
4	157	12.94	5	165.2	12.51	5	ns	128.4	6.55	5	124.4	12.49	5	ns
8	179.3	14.33	5	187.9	12.61	5	ns	139.4	5.04	5	138.3	13.94	5	ns
11	194.5	12.48	5	206.2	12.18	5	ns	148.1	4.67	5	146.7	15.8	5	ns
14	210.8	10.86	5	222.2	13.79	5	ns	156.1	2.28	5	154.3	16.76	5	ns

		Control (Male)			NBD-PMX (Male)				Control (Female)			NBD-PMX (Female)			
		Mean	**SD**	**n**	**Mean**	**SD**	**n**		**Mean**	**SD**	**n**	**Mean**	**SD**	**n**	
Hb (g/dL)	Day 3	13.1	0.47	10	13.2	0.46	6	ns	13.7	0.25	4	13.6	0.45	9	ns
	Day 15	14	0.24	4	14.1	0.45	5	ns	14.2	0.78	5	14.5	0.71	5	ns
WCC (10^9/L)	Day 3	3.4	0.87	10	3.3	1.18	6	ns	2.9	0.79	4	2.7	0.6	9	ns
	Day 15	5.7	1.42	4	4.5	1.9	5	ns	3.7	1.27	5	5.2	0.55	5	*
Plt (10^9/L)	Day 3	1037	94.7	10	907	102.3	6	*	1009	113.7	4	1063	59.4	9	ns
	Day 15	953	77	4	958	53.1	5	ns	1000	123.1	5	1024	78.3	5	ns
PT (s)	Day 3	22.5	0.69	8	22.4	0.7	8	ns	21.7	1.16	4	21.6	1.3	10	ns
	Day 15	22.6	0.73	5	22.3	0.52	5	ns	24.5	0.79	5	24.7	0.98	5	ns
Fibrinogen (g/L)	Day 3	1.58	0.076	8	1.56	0.086	8	ns	1.52	0.057	4	1.56	0.052	10	ns
	Day 15	1.59	0.063	5	1.64	0.073	5	ns	1.4	0.076	5	1.39	0.09	5	ns
Urea (mmol/L)	Day 3	5.6	1.01	10	5.8	0.42	10	ns	4.8	0.83	10	6	1.06	10	**
	Day 15	7.2	1.15	5	7.2	1.54	5	ns	6.4	0.68	5	5.9	1.08	5	ns
Hcre (µmol/L)	Day 3	17	1.1	10	17	1.6	10	ns	16	1.3	10	17	1.0	10	*
	Day 15	21	1.5	5	21	2.8	5	ns	21	1.1	5	20	1.2	5	ns
Na (mmol/L)	Day 3	140	1.3	10	140	1.4	10	ns	140	1.4	10	140	1.8	10	ns
	Day 15	140	1.6	5	140	0.8	5	ns	140	1.1	5	140	1.6	5	ns
K (mmol/L)	Day 3	3.6	0.11	10	4	0.45	10	**	3.7	0.21	10	3.6	0.26	10	ns

	Day 15	3.9	0.16	5	3.6	0.18	5	*	3.5	0.22	5	3.5	0.13	5	ns
AST (IU/L)	Day 3	73	11.5	10	75	11.9	10	ns	71	10.8	10	71	8.5	10	ns
	Day 15	49	6.2	5	56	8.4	5	ns	76	25	5	65	5.1	5	ns
ALT (IU/L)	Day 3	61	10.5	10	69	7.5	10	ns	47	8.9	10	53	12.7	10	ns
	Day 15	38	7.1	5	41	8.7	5	ns	35	8.7	5	31	9.8	5	ns
Glucose (mmol/L)	Day 3	6.4	0.66	10	6.7	1.47	10	ns	5.5	0.84	10	6	1.41	10	ns
	Day 15	9.5	2.42	5	7	0.58	5	**	5.5	0.99	5	5.8	0.55	5	ns
Total Protein (g/L)	Day 3	53	1.9	10	54	1.3	10	ns	54	3	10	56	1.7	10	ns
	Day 15	57	1.4	5	59	2.4	5	ns	59	3.4	5	58	1.8	5	ns
Albumin (g/L)	Day 3	36	2.2	10	38	1.8	10	*	39	2.7	10	39	2.4	10	ns
	Day 15	40	2.3	5	42	1.9	5	ns	42	3.5	5	42	2.1	5	ns
Cholesterol (mmol/L)	Day 3	2.9	0.39	10	2.7	0.36	10	ns	2.9	0.58	10	3.1	0.61	10	ns
	Day 15	2.3	0.37	5	2.5	0.81	5	ns	1.8	0.41	5	1.9	0.29	5	ns

Hb: Haemoglobin, WCC: total white cell count, Na: Sodium, K: Potassium, Plt: Platelet count, PT: Prothombin Time, ALT: Alanine Aminotransferase, AST: Aspartate Aminotransferase, Hcre: Enzymatic Creatinine.

Table S1: No significant changes in weight, haematological, coagulation or clinical chemistry parameters. Analysis by two-sample t-test; ns=not significant, *=p<0.05, **=P<0.01. Where significances were found the data was within the historical control ranges these changes were considered not to be of toxicological significance.

Conditions / Timepoint	Freezer -20 °C			
	RT / min	Conc. / µg per 5mL (Δ%)	Total imp. RRT(%)	pH
0	6.538 -	60.51 -	ND ND	7.5 -
48h	6.539 6.539	56.56 (6.5%) 56.18 (7.2%)	ND ND	7.5 7.5
1m	6.548 6.549	55.0 (9.1%) 53.44 (11.6%)	ND ND	7.5 7.5
3m	6.515 6.517	57.23 (5.4%) 49.44 (18%)	ND ND	7.5 7.5
5m	6.517 6.519	65.01 (7.4%) 61.58 (1.8%)	ND ND	7.5 7.5
6m	6.538 6.537	62.17 (2.7%) 61.59 (1.8%)	ND ND	7.5 7.5
10m	6.514 6.508	57.85 (4.4%) 55.43 (8.4%)	ND ND	7.5 7.5
18m	6.519 6.520	65.66 (+8.5%) 65.90 (+8.9%)	ND ND	7.5 7.5
24m	6.456 6.490	60.53(+0.03%) 57.00 (-5.8%)	ND ND	7.5 7.5

Table S2: NBD-PMX is stable in aqueous formulation over 24 months. Summary table of stability as assess by HPLC over 10 months stored under GMP frozen conditions (-20^{0}C). Data shown in blue is representing "inverted" position vials;.Δ% is relative to time zero. Acceptance criteria for the GMP product**:** Retention time (RT) for NBD-PMX as 6.50 min (Range 6.30-6.75 min). HPLC assay concentration for technical batch is as 60.51µg/5mL (+/-25%). Total impurities – report as RRT (%) for each impurity. pH 7.5 (7.0-8.0).

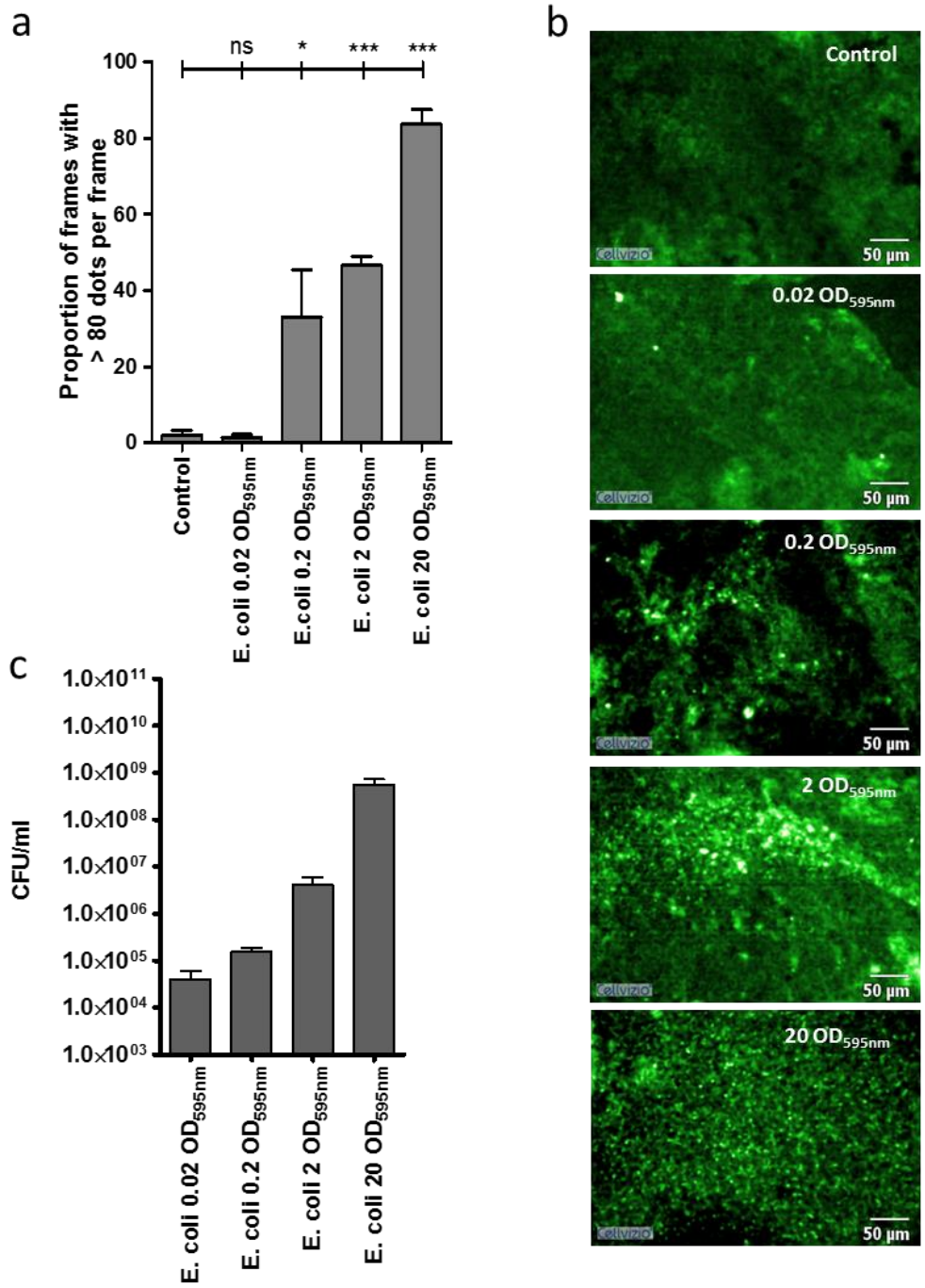

Figure S5: OEM coupled with NBD-PMX enables bioburden evaluation in the distal ovine lung. a) Proportion of positive frames for *E. coli* presence with increasing concentrations of bacteria with NBD-PMX instilled topically and imaged. n=3 for all conditions, bars represent mean (+/-SEM), analysis by students-t test, ns=not significant, *=p<0.05, ***=p<0.001, all analyses when compared to control segment. b) Representative images for each bacterial concentration and c) Bacterial yields from bacteria retrieved on lavage, confirming the increasing concentration of bacteria per pulmonary segment, n=3 for each concentration.

Patient	**D1**	**D2**	**D3**	**D4**	**D5**	**D6**
Gender	F	F	F	M	F	M
Age	62	58	66	68	68	68
FEV1 (% predicted)	2.46 (98%)	1.54 (81%)	1.35 (66%)	1.32 (39%)	1.54 (76%)	2.75 (94%)
Bronchiectasis Location (CT scan) and Type	Tubular bronchiectasis, all lobes	Varicose bronchiectasis LUL and LLL. Tubular in other lobes	Tubular bronchiectasis in all lobes	Tubular bronchiectasis in all lobes	Tubular bronchiectasis in RLL and RML	Tubular bronchiectasis in RML and Lingula
OEM Imaging and NBD-PMX Administration	RML	LLL	RLL	RML	RML	RML
Hb (g/L) Pre-Bronchoscopy	-*	131	139	144	107	140
Hb (g/L) Post-Bronchoscopy	151	129	141	138	104	139
WCC (10^9/L) (109/L) Pre-Bronchoscopy	-*	5.9	338	8.5	5	9.6
WCC (10^9/L) Post-Bronchoscopy	15.8	9.9	350	13.3	8.4	11
Platelets (10^9/L) Pre-Bronchoscopy	-*	394	313	295	390	234
Platelets (10^9/L) Post-Bronchoscopy	246	410	314	305	381	222
Sodium (mmol/L) Pre-Bronchoscopy	137	137	144	141	141	140
Sodium (mmol/L) Post-Bronchoscopy	139	139	141	142	139	135
Potassium (mmol/L) Pre-Bronchoscopy	4.4	4.8	4	4	4.2	3.3
Potassium (mmol/L) Post-Bronchoscopy	4	4.3	3.9	3.6	3.8	3.4
Urea (mmol/L) Pre-Bronchoscopy	3.8	6.4	5.9	6	5.8	9.9
Urea (mmol/L) Post-Bronchoscopy	3.4	6.1	6.1	6.4	5.8	10.6
Creatinine (µmol/L) Pre-Bronchoscopy	60	66	72	92	63	110
Creatinine (µmol/L) Post-Bronchoscopy	59	74	68	89	59	124
Bilirubin (µmol/L) Pre-Bronchoscopy	7	7	7	10	7	23
Bilirubin (µmol/L) Post-Bronchoscopy	8	7	7	8	6	22
ALT (U/L) Pre-Bronchoscopy	19	15	22	33	16	38
ALT (U/L) Post-Bronchoscopy	17	15	24	30	15	41
C-reactive Protein (mg/L) Pre-Bronchoscopy	<1	3	5	2	<1	30
C-reactive Protein (mg/L) Post-Bronchoscopy	<1	3	5	2	<1	30
	*= Insufficient Sample, Hb= Haemoglobin, WCC= White cell count, ALT= Alkaline Transferase LUL- Left upper lobe, LLL- Left lower lobe, RLL- Right lower lobe, RML- Right middle lobe					
Total Procedure Time (mins)	33	22	25	18	25	20
NBD-PMX Administration to End Procedure Including BAL (mins)	22	11	13	12	7	7
Total Number of Passes with OEM	4	3	3	5	4	5
Serious Adverse Events	None	None	None	None	None	None
Adverse Events	None	Mild Sore Throat	None	None	Mild Fever & New Infiltrate on chest radiograph (resolved)	Increased Sputum production
BAL/Sputum Growth	*S. aureus*	*P. aeruginosa*	*S. pneumoniae*	*P. miribalis*	*P. aeruginosa*	*S. pneumoniae/H. influenzae*
CFU/ml	2.8×10^5	1.7×10^5	8×10^5	2.7×10^6	2.1×10^4	$2.2 \times 10^5/3 \times 10^4$

Table S3: Bronchiectasis patient demographics, blood results, adverse events and microbiological growth.

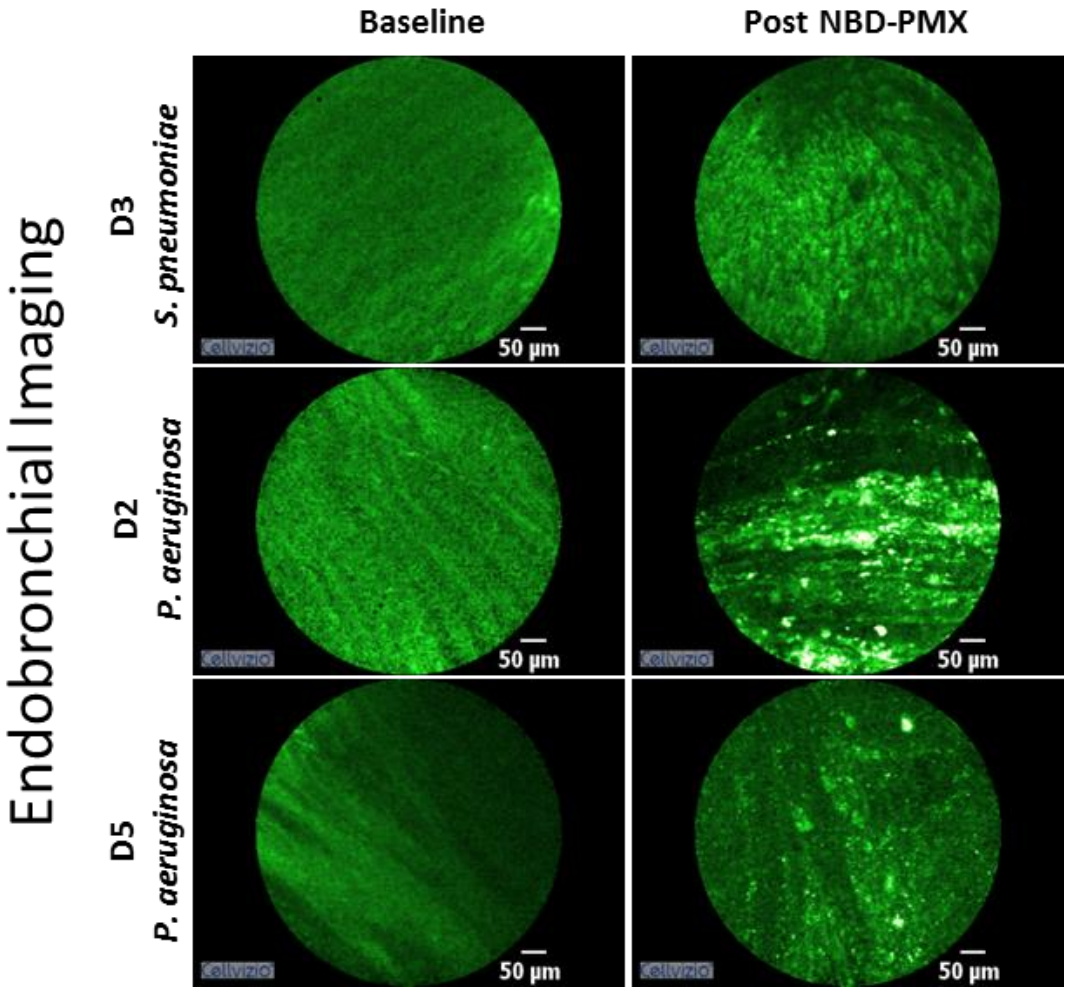

Figure S6: NBD-PMX labels gram-negative bacteria endobronchially. Representative images of bronchial structures demonstrating baseline (left) and following NBD-PMX administration *in vivo*. Bacterial presence, often in clumps, can be seen in patients with gram-negative bacteria (D2 and D5) but not seen in the patient with gram-positive bacteria (D3).

Patient	**D7**	**D8**	**D9**	**D11**	**D12**	**D13**
Gender	M	F	F	M	M	M
Age	72	72	71			
Primary diagnosis necessitating ICU admission	Post-operative care following oesophageal carcinoma surgery	Post-operative care following perforated gastric ulcer, re-admission with respiratory failure	Poly-trauma, pedestrian in road traffic accident	Respiratory failure secondary to pneumonia	Respiratory failure secondary to pneumonia	Respiratory failure, fluid overload and suspected pneumonia
Length of Time in ICU (days from admission to procedure)	9	3*	6	1	10	3
APACHE II Score (0-71)	12	24	14	21	24	31
Hospital Mortality Probability Score (%)	11.8	65.7	7.2	38.9	32.5	73.3
Imaging changes (CT scan or chest radiograph)	CT: RUL and RLL	Chest radiograph: RLL and LLL	Chest radiograph: LLL	Chest radiograph: RLL	CT: RML and RLL changes. Cavitation RML	Chest radiograph: RLL, RML, LLL and L effusion
OEM imaging and NBD-PMX administration	RLL	LLL	LLL	RLL	RLL	RML
Total procedure time (mins)	14	13	19	16	14	12
NBD-PMX administration to end procedure including BAL (mins)	4	7	10	11	12	8
Total number of passes with OEM	4	4	4	8	5	4
Adverse Events	Fever (unrelated)	None	None	None	Haemoptysis (minor)	None
Serious Adverse Events	Laparotomy for leaking jejunostomy (unrelated)	None	None	None	None	None
	*Re-admission to ICU following initial 23 day ICU stay LUL- Left upper lobe, LLL- Left lower lobe, RUL- Right upper lobe					
Hb (g/L) Pre-Bronchoscopy	101	77	85	145	125	81
Hb (g/L) Post-Bronchoscopy	97	77	81	132	114	86
WCC (10^9/L) (109/L) Pre-Bronchoscopy	23.4	14.6	8.4	11.9	11.5	5.4
WCC (10^9/L) Post-Bronchoscopy	25.8	13.9	8.6	14.1	11.4	7
Platelets (10^9/L) Pre-Bronchoscopy	409	496	146	278	209	115
Platelets (10^9/L) Post-Bronchoscopy	398	494	186	259	201	137
Sodium (mmol/L) Pre-Bronchoscopy	137	138	149	145	138	136
Sodium (mmol/L) Post-Bronchoscopy	135	136	148	144	137	136
Potassium (mmol/L) Pre-Bronchoscopy	4.4	4.6	4.0	3.2	4.2	4.3
Potassium (mmol/L) Post-Bronchoscopy	4.3	4.9	4.1	3.6	3.4	4.6

Urea (mmol/L) Pre-Bronchoscopy	4.1	10.6	7.1	5.7	8.3	10.3
Urea (mmol/L) Post-Bronchoscopy	4.0	10.5	7.9	6.2	8.7	9.2
Creatinine (µmol/L) Pre-Bronchoscopy	52	87	59	57	47	138
Creatinine (µmol/L) Post-Bronchoscopy	53	85	58	55	50	121
Bilirubin (µmol/L) Pre-Bronchoscopy	14	7	14	11	38	8
Bilirubin (µmol/L) Post-Bronchoscopy	15	6	14	9	30	7
ALT (U/L) Pre-Bronchoscopy	17	17	86	49	42	18
ALT (U/L) Post-Bronchoscopy	18	19	169	44	36	17
C-reactive Protein (mg/L) Pre-Bronchoscopy	416	173	81	ND	27	62
C-reactive Protein (mg/L) Post-Bronchoscopy	416	164	90	53	24	ND
	Hb= Haemoglobin, WCC= White cell count, ALT= Alkaline Transferase, ND= not done					
BAL Growth (Bacterial)	No growth	*S. maltophilia*	*P. aeruginosa*	*K. oxytoca*	No growth	Coagulase-negative *S. epidermidis* (respiratory tract commensal)
CFU/ml	-	1×10^4	1×10^2 (under VAP diagnostic threshold)	2×10^2	-	7×10^2
Animicrobial therapy prior to procedure	Metronidazole, Ciprofloxacin, Vancomycin and Fluconazole (anti-fungal)	None	None	Temocillin	Flucloxicillin and amoxicillin/clavulanic acid	Ceftriaxone and clarythromycin
Growth of other organisms from BAL	-	-	-	Candida albicans (moderate numbers)	Candida albicans (small numbers)	-
OEM Diagnosis	Pneumonia (VAP)	Atelectasis, No VAP	No VAP	Pneumonia	Pulmonray Abscess	Atelectasis, No VAP

Table S4: ICU patient demographics for six patients included in the analysis, blood results, adverse events and microbiological growth.

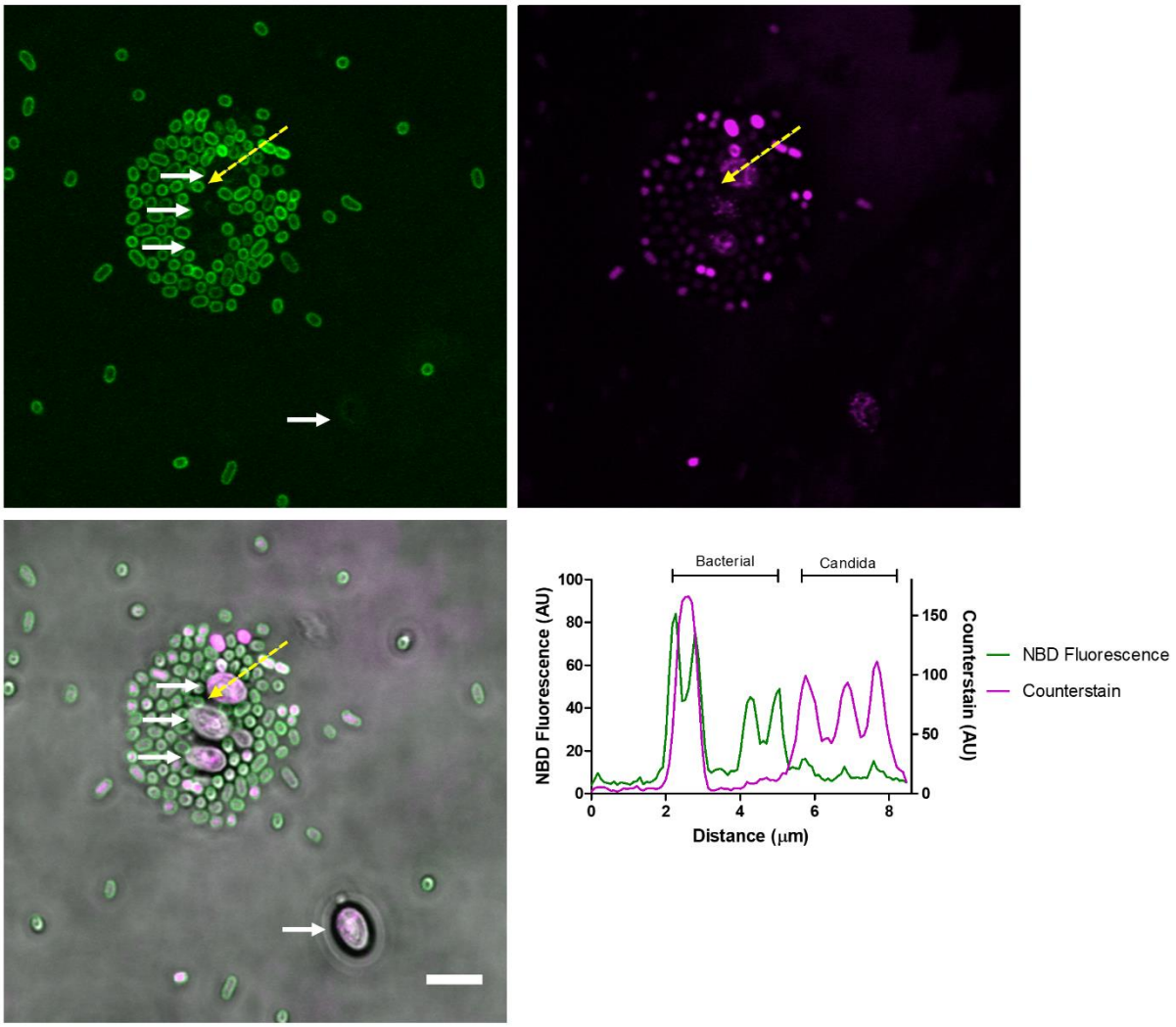

Figure S7: Ex-vivo confocal labelling of species from BAL in patient D11. Confocal images of bacteria and fungi isolated from BALF of patient D11 (identified as *K. oxytoca* and *C. albicans*) in co-culture in the presence of NBD-PMX (10µM). Upper left image shows NBD-PMX fluorescence of *K. oxytoca* labeling but none of *C. albicans* (white arrows). Upper tight image shows counterstain and lower left panel demonstrates merge, scale bar 5 µm. Plot profile along yellow dashed line demonstrates labeling with counterstain but not NBD-PMX of Candida.

Supplementary Methods:

Haemolysis Assay: Erythrocytes were isolated from freshly drawn, anticoagulated human blood and resuspended to 20 vol % in PBS. In a 96-well microtiter plate, 100 µl of erythrocyte suspension was added to 100 µl of NBD-PMX at various concentrations. PBS acted as negative control and 0.2% Triton X-100 acted as positive control. The plate was incubated at 37°C for 1 h, each well was diluted with 150 µl of PBS and the plate centrifuged at 1,200g for 15 min. 100µl of the supernatant from each well was transferred to a fresh microtiter plate, and absorbance at 350 nm was measured in a Synergy H1 Multi-Mode Spectrophotometer (BioTek, VT, US). Data is expressed as % of positive control.

Murine intra-tracheal administration: Adult male CD-1 mice aged 8-12 weeks were given a single dose of NBD-PMX (100µg) in 50µl PBS or PBS vehicle control via direct intra-tracheal administration. Animals were monitored for clinical signs, weighed regularly and then sacrificed at 48 hours or 14 days (n=3 per group per time point). Following necroscopy, cellular infiltrate into the lung was assessed by harvesting bronchoalveolar lavage fluid (BALF) via 3 x 0.8ml PBS flushes of the lung and cytospin slides were prepared and stained with Diff-Quick (Thermo Fisher Scientific). Cell types were quantified using a light microscope. Lung, liver and kidney were taken for histopathological assessment, fixed and stained with haematoxylin and eosin.

Surfactant Constituent Synthesis: Surfactant 5µg 1,2-Dipalmitoyl-sn-glycero-3-phosphocholine (DPPC) and 2.5µg L-α-Phosphatidyl-DL-glycerol sodium salt (from egg yolk lecithin; PG) were dissolved in 500µl chloroform and evaporated under nitrogen to a thin lipid film in a round bottom flask. The lipid film was rehydrated with PBS at 48°C for 1 hour with agitation (750rpm) to generate multilammelar vesicles (MLV) and diluted 1:4 for use in confocal experiments.

Chemical Synthesis of NBD-PMX: The NBD-PMX probe was synthesised from its precursor Polymyxin B sulfate in five steps (Scheme 1). The probe was synthesized using reported methods (49) with moderate modifications. The fluorophore was incorporated via an amide bond coupling using the NHS ester of the NBD-PEG2-OH and the tetra-boc protected polymyxin **C**. NBD-PMX was obtained after the TFA cleavage and HPLC purification.

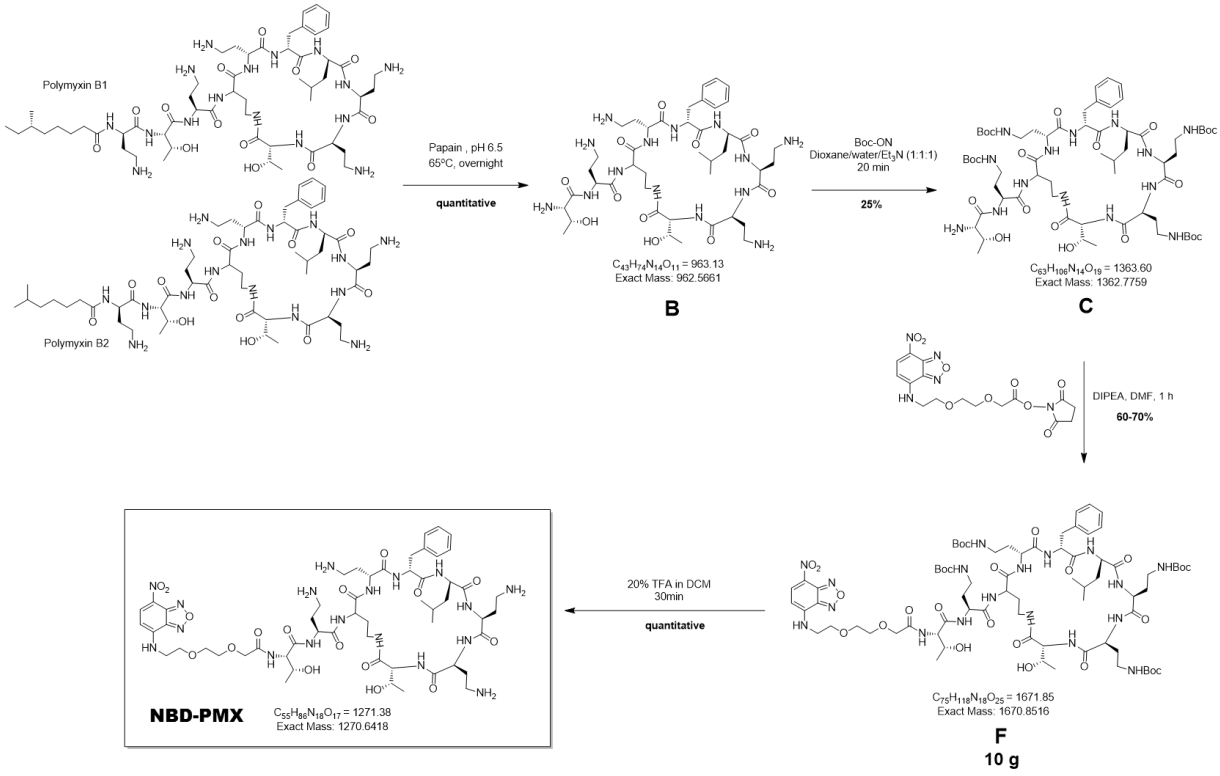

Scheme 1. Synthetic route of NBD-PMX probe.

Experimental Procedure

Step 1: Preparation of B: Polymyxin B sulfate (10 g, 7.7 mmol, 1 eq) was dissolved in deionized water (200 mL) at a pH of 6.5 (use HCl aq solution to adjust the pH). Papain (1.5 g) was dissolved in water (25 mL) (same pH). The solutions were combined and toluene (0.5 mL) was added, and the mixture was gently stirred at 65 °C overnight. The mixture was then stirred in boiling water for 5 min and the precipitate formed (denatured papain) was removed by centrifugation and filtration. The filtrate was concentrated *in vacuo* and freeze dried to give the crude product **B** in quantitative yield. This step was carried forward to the next step without any further purification. MS *m/z* 963.2 (100%, $[M+H]^+$).

Step 2: Preparation of C: Crude **B** (5.5 g, 5.7 mmol, 1 eq) was dissolved in a mixture of H_2O: Dioxane: Et_3N (150 mL, 1:1:1) and Boc-ON (4.52 g, 17.1 mmol, 3eq) was added. The solution was stirred for 20 min at room temperature and then quenched with methanolic ammonia (20 mL, 2M ammonia in MeOH). The reaction was followed up by ELSD. Solvents were evaporated and the resulting mixture

was subjected to silica gel chromatography column (MeOH: DCM, 15:85) to afford white solid **B** (1.7 g, 22%). MS *m*/*z* 1363.7 (100%, $[M+H]^+$).

***Step 3: N*-(4-Nitrobenz-2-oxa-1,3-diazol-7-yl)amino-3,6-dioxaoctanoic acid (NBD-PEG$_2$-OH)**: DIEA (850 µl, 5.00 mmol) and solid 8-Amino-3,6-dioxaoctanoic acid (H_2N-PEG_2-OH) (392 mg, 2.40 mmol, 1 eq) were added slowly, over an hour, to a solution of NBD-Cl (401 mg, 2.01 mmol) in methanol (20 mL) at 0°C. The reaction mixture was stirred overnight at room temperature. The solvent was evaporated and the remaining material was purified by chromatography on silica with DCM/MeOH (8:2) as the eluent to give NBD-PEG2-OH (400 mg, 1.23 mmol, 51%) as dark red oil. ^{1}H NMR (500 MHz, DMSO): δ 10.9 (s, 1H; COOH), 8.49 (d, *J* = 8.5 Hz, 1H; CH NBD), 7.1 (s, 1H, NH), 6.23 (d, *J* = 8.5 Hz, 1H; CH NBD), 4.25 (s, 2H), 3.93 (t, *J* = 5.3 Hz, 2H; CH_2), 3.80 (s, 4H), 3.72 (t, *J* = 6.8 Hz, 2H; CH_2) ppm; MS (ESI-): m/z calcd for $C_{12}H_{14}N4O_7$ [M-H]: 325.1; found: 325.2

***N*-(4-Nitrobenz-2-oxa-1,3-diazol-7-yl)amino-3,6-dioxaoctanoic acid, succinimidyl ester (NBD-PEG$_2$-NHS):** To a solution of NBD-PEG_2-OH (2.4 g, 7.4 mmol, 1 eq) in anhydrous DCM (500 mL) was added EDC·HCl (1.56 g, 8.18 mmol, 1.1 eq) and DIPEA (1.36 mL, 10 mmol). After stirring the mixture for 10 min, *N*-hydroxysuccinimide (0.94 g, 8.18 mmol) was added and allowed to stir for 16 h. The reaction mixture was diluted with DCM (250 mL) and treated with 5% aqueous citric acid (2 x 200 mL), sat. aqueous $NaHCO_3$ and brine. The organic layer was dried over Na_2SO_4, filtered and reduced *in vacuo* to afford product as dark brown solid (1.0 g, quantitative). The crude was used for next step without further purification.

Step 4: Preparation of F: A solution of NBD-PEG_2-NHS (466 mg, 1.1 mmol, 1 eq), DIPEA (384 µL, 2.2 mmol, 2 eq) and amine **C** (1.5 g, 1.1 mmol, 1 eq) in DMF (150 mL) was stirred at room temperature for 1 h and protected from light. After completion of the reaction (TLC), volatiles are removed under vacuum. The crude mixture was purified by flash chromatography (DCM : MeOH, 90:10) to afford dark orange/brown solid (1.2 g, 65%). HPLC (254nm & 495nm) Rt = 7.80 min; *m*/*z* 1671.7 (25%, $[M+H]^+$); 1693.9 (65%, $[M+Na]^+$).

Step 5: *Preparation of* NBD-PMX: A solution of boc-protected polymyxin **F** (150 mg, 0.09 mmol) in 20% TFA in DCM (2 mL) was vigorously stirred for 45 min at room temperature and protected from light. The reaction mixture was evaporated in *vacuo* and the resultant was dissolved in ether. Ether layer was decanted after centrifugation (3 × 2 mL). The resultant yellow/brown solid (40 mg, quantitative) was dried under vacuum. The crude product was purified by preparative HPLC in MeOH/H_2O as gradient solvent system with 0.1% formic acid as an additive. The fractions collected from prep-HPLC were freeze dried to afford red/orange solid (30 mg, 26% recovery from HPLC).

Characterization: For analytical HPLC, a Poroshell 120 SB-C18, 2.7 µm, 4.6 x 50mm column was used with a diode array detector. For prep-HPLC method: Discovery C18 reverse-phase column (5 cm x 4.6 mm, 5 µm) with a flow rate of 1 mL/min and eluting with H_2O/MeOH/HCOOH (95/5/0.05) to H2O/MeOH/HCOOH (5/95/0.05), over 6 min, holding at 95% MeOH for 4 min, with detection at 254 and 495nm and by ELSD. HPLC (495nm): Rt = 4.1 min; MS *m/z* 1271.7 (95%, $[M+H]^+$); 1293.7 (100%, $[M+Na]^+$); FTMS calc. 636.3282 $([M+2H]/2)^+$, found 636.3344.

FTMS

Molecular formula: $C_{55}H_{96}N_{19}O_{17}$

Major peak detected: 636.3344 (*m/z*: 2)

Absorption / Emission: 467 nm / 539 nm.

Solubility: Fully soluble in water.

Stability: stable at room temperature for > than 1 week.

Storage: Stored at -20 °C under inert atmosphere. Protect from light.

Analytical HPLC of NBD-PMX

```
Data File C:\CHEM32\1\DATA\JUL 2013\ELSD  2013-08-02  9576\041-0201.D
Sample Name: BAC2-STABILITY

================================================================
Acq. Operator   : MARC                          Seq. Line :   2
Acq. Instrument : Instrument 1                   Location : Vial 41
Injection Date  : 02/08/2013 06:48:33 PM              Inj :   1
                                                Inj Volume : 10 µl
Acq. Method     : C:\CHEM32\1\DATA\JUL 2013\ELSD  2013-08-02  9576\BAC2-STABILITY-010813.M
Last changed    : 02/08/2013 06:31:29 PM by MARC
Analysis Method : C:\CHEM32\1\DATA\JUL 2013\ELSD  2013-08-02  9576\041-0201.D\DA.M (BAC2-
                  STABILITY-010813.M)
Last changed    : 02/08/2013 06:31:29 PM by MARC
Method Info     :
                  DISCOVERY-C18,
                  BAC-2 stability(GE10CM5U): 5 TO 95% MeOH+0.1% formic acid in water+0.1%FA
                  in 6min, 1 min to 5% MeOH  and then 2min isocratic
```

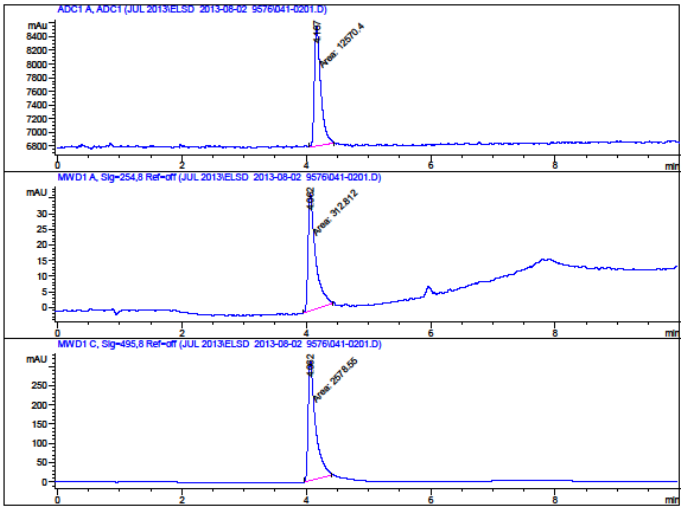

HRMS of NBD-PMX